Open research issues on Modeling, Simulation and Optimization in Electrical Systems

M. Panoiu [1], F. Neri [2]
[1] Department of Electrical Engineering and Industrial Informatics, University Polytehnica Timisoara – Hunedoara, Romania
[2] Department of Computer Science, University of Naples "Federico II", Naples, ITALY
manuela.panoiu@upt.ro, nerifil@gmail.com

Abstract - We are going to present here a number of results on open research issues in the area of Modeling, Simulation and Optimization in Electrical Systems. The results range from methodologies to applications and include: power quality problems in electronic converters, control of power in complex computing environment, optimization methods for power control systems.

Keywords - Modeling and simulation of electrical systems and machines, Modeling and simulation of power electronics.

Introduction

The special Issue "Modeling, Simulation and Optimization in Electrical Systems" intends to collect original unpublished papers, aiming theoretical and practical matters, dealing with recent trends of Modeling, Simulation and Optimization in Electrical Systems.

The power quality problems are generated by many applications of static power electronic converters, fluorescent lamps, arc furnaces and so on. One of the papers from this special issue studies the current harmonic spectrum generated by functioning of an electrothermal installation with electromagnetic induction. In order to analyze the electrical parameters that characterize the electrothermal installation functioning, measurement sets were accomplished using two methods. The first method consists in using a power and energy quality analyzer and the second method uses an acquisition system that contains an adapting interface and a data acquisition board connected to a computer. Paper contains also a simulation of the electrothermal installation functioning realized in PSCAD-EMTDC.

The proliferation of nonlinear electronic loads is increasing day by day, and it can anticipate an influx of newer technologies in this domain in the future. Another article focuses on the impacts of various home nonlinear electric equipment on the power quality of electrical distribution system. It was studied the influence of operating mode on the harmonic pollution generated by nonlinear home appliances operating in an isolated mode, using the *CA 8334B* three-phase power quality analyzer. Although home electric appliances are low power receivers, the cumulative effect produced by a large number of small harmonic sources can be substantial.

Cloud *computing*, as a new model of service provision in distributed computing environment, faces the great challenge of energy consumption because of its large demand for computing resources. Choosing improper scheduling method to execute cloud workflow tends to result in the waste of power consumption. In order to lower the higher power consumption for cloud workflow executing, we propose a power consumption optimization algorithm for cloud workflow scheduling based on SLA (Service Level Agreement), which can reduce power consumption while meeting the performance-based constraints of time and cost. The algorithm first searches for all feasible scheduling solutions of cloud workflow application with critical path, then the optimal scheduling solution can be found out through calculating total energy consumption for each feasible scheduling solution. The experimental results show that compared with traditional workflow scheduling algorithms based on QoS, the optimization algorithm proposed in this paper not only meets the constraints of time and cost defined in SLA, but also reduces the average power consumption by around 10%.

In one of the papers, the assessment of new coordinated design of Power System Stabilizers (PSSs) and Static Var Compensator (SVC) in a multimachine power system via statistical method is proposed. The coordinated design problem of PSSs and SVC over a wide range of loading conditions is handled as an

optimization problem. The Bacterial Swarming Optimization (BSO), which synergistically couples the Bacterial Foraging (BF) with the Particle Swarm optimization (PSO), is employed to seek for optimal controllers parameters. By minimizing the proposed objective function, in which the speed deviations between generators are involved; stability performance of the system is enhanced. To compare the capability of PSS and SVC, both are designed independently, and then in a coordinated manner. Simultaneous tuning of the BSO based coordinated controller gives robust damping performance over wide range of operating conditions and large disturbance in compare to optimized PSS controller based on BSO (BSOPSS) and optimized SVC controller based on BSO (BSOSVC). Moreover, a statistical T test is executed to validate the robustness of coordinated controller versus uncoordinated one.

Conclusions

Harmonic analyzing is very necessary for designing the electronic devices which must compensate the distorted regime introduced into the power system by the nonlinear loads. Using PSCAD-EMTDC simulations of the electric equipments functioning can be accomplished. So, the command and control elements for the electrothermal installation were modeled. The PSCAD EMTDC is able to display the variation of the current harmonics. Acquisition with CA8334B power analyzer represents a very practical method for studying in real time of the electrical parameters variation.

Most of the nonlinear electric equipment highly distorted current waveforms which produces high levels of harmonic distortions when connected to a distribution system. *SMPS* is present in almost all home and commercial nonlinear loads, such as computers, monitors, laptops, electronic ballasts for fluorescent lamps, etc. From all house nonlinear electric equipment, these type of loads show the most current harmonic distortion. *SMPS*'s current has a significant amount of multiply 3^{rd} harmonics order (3^{rd}, 9^{th}, 15^{th}, etc.). These harmonics add algebraically through neutral conductor. So, in three-phase power systems that have a neutral conductor and a large number of single-phase *SMPS* loads, even if the loads are balanced (on the three phases), will circulate an important neutral current, that can not be eliminated or reduced.

Current harmonic distortion is influenced by operation mode for almost analysed nonlinear loads, with the exception of the microwave oven.

Induction heat plate generates harmonics only in stand-by mode, the laser printer only in idle mode and the air condition devices, especially in stand-by mode. Due to the nonlinear electronics equipment show that harmonic voltage distortion is up 4.9 %.

The cumulative effect produced by a large number of small nonlinear electric equipment (harmonic sources) can be substantial, because the total harmonic distortion current (THDI) can reach up to 130% at the terminals of these electric loads, generating additional power and energy losses in electric networks.

Through analyzing the energy computing model for cloud workflow execution, we have proposed an energy consumption algorithm of cloud workflow scheduling under the constraints of time and cost in SLA. Simulated experiments demonstrate that this optimization method is fully effective and feasible. But the energy optimization issue isn't implemented in the virtual cloud environment. So, we will further investigate the energy consumption optimization of cloud workflow scheduling based on the virtual machines allocation in the future, and carry out experiments in real virtualization cloud platform so as to ensure the correctness and effectiveness of research result

The statistical assessment of the robust coordinated design of PSSs and SVC damping controller in a multimachine power system is proposed in this paper. The design problem of the proposed controller is formulated as an optimization problem and BSO is employed to search for optimal controller parameters. By minimizing the time domain objective function, in which the deviations in speed are involved; stability performance of the system is improved. Simulations results assure the effectiveness of the proposed coordinated controller in providing good damping characteristic to system oscillations over a wide range of loading conditions and large disturbance. Moreover, it is superior to uncoordinated controller through the statistical assessment.

Finally before diving into the collected research works [17-21], let us remember the reader that WSEAS Transactions on Systems has been hosting and will continue to do so a few Special Issues in the latest years [1-20]. This is has the objective of creating an active and contributing research community around the journal and to present their latest efforts which have achieved wide interest among its members. As a reader of the journal you are invited to take inspiration by the presented papers and to consider to submit your future works to the journal itself.

Enjoy your reading!

References

[1] Hajek, P., Neri, F. (2013). An introduction to the special issue on computational techniques for trading systems, time series forecasting, stock market modeling, financial assets modelling. WSEAS Transactions on Business and Economics, 10 (4), pp. 201-292.

[2] Azzouzi, M., Neri, F. (2013). An introduction to the special issue on advanced control of energy systems (2013) WSEAS Transactions on Power Systems, 8 (3), p. 103.

[3] Bojkovic, Z., Neri, F (2013). An introduction to the special issue on advances on interactive multimedia systems. WSEAS Transactions on Systems, 12 (7), pp. 337-338.

[4] Pekar, L., Neri, F. (2013). An introduction to the special issue on advanced control methods: Theory and application. WSEAS Transactions on Systems, 12 (6), pp. 301-303.

[5] Guarnaccia, C., Neri, F. (2013). An introduction to the special issue on recent methods on physical polluting agents and environment modeling and simulation WSEAS Transactions on Systems, 12 (2), pp. 53-54.

[6] Neri, F. (2012). An introduction to the special issue on computational techniques for trading systems, time series forecasting, stock market modeling, and financial assets modeling WSEAS Transactions on Systems, 11 (12), pp. 659-660.

[7] Muntean, M., Neri, F. (2012). Foreword to the special issue on collaborative systems WSEAS Transactions on Systems, 11 (11), p. 617.

[8] Pekar, L., Neri, F. (2012). An introduction to the special issue on time delay systems: Modelling, identification, stability, control and applications WSEAS Transactions on Systems, 11 (10), pp. 539-540.

[9] Volos, C., Neri, F. (2012). An introduction to the special issue: Recent advances in defense systems: Applications, methodology, technology. WSEAS Transactions on Systems, 11 (9), pp. 477-478.

[11] Doroshin, A. V., Neri, F. (2014) Open research issues on Nonlinear Dynamics, Dynamical Systems and Processes. WSEAS Transactions on Systems, 13, in press.

[12] Ciufudean, C., Neri, F. (2014) Open research issues on Multi-Models for Complex Technological Systems. WSEAS Transactions on Systems, 13, in press.

[13] Neri, F. (2014) Open research issues on Computational Techniques for Financial Applications. WSEAS Transactions on Systems, 13, in press.

[14] Karthikeyan, P., Neri, F. (2014) Open research issues on Deregulated Electricity Market: Investigation and Solution Methodologies. WSEAS Transactions on Systems, 13, in press.

[15] Panoiu, M., Neri, F. (2014) Open research issues on Modeling, Simulation and Optimization in Electrical Systems. WSEAS Transactions on Systems, 13, in press.

[16] Neri, F. (2014) Open research issues on Advanced Control Methods: Theory and Application. WSEAS Transactions on Systems, 13, in press.

[17] Rob, R., Panoiu, C., Iordan, A., Harmonic Analysis in Functioning of an Electrothermal Installation with Electromagnetic Induction, WSEAS Transactions on Systems, 13, in press

[18] Ali, E. S, Abd-Elazim, S. M, Stability Enhancement of Multimachine Power System via New Coordinated Design of PSSs and SVC, WSEAS Transactions on Systems, 13, in press

[19] Iagar, A., Popa, G.N., Dinis, C., The influence of home nonlinear electric equipment operating modes on power quality, WSEAS Transactions on Systems, 13, in press

[20] Yonghong Luo, Shuren Zhou, Power Consumption Optimization Strategy of Cloud Workflow Scheduling based on SLA, WSEAS Transactions on Systems, 13, in press

Harmonic Analysis in Functioning of an Electrothermal Installation with Electromagnetic Induction

RALUCA ROB, CAIUS PANOIU, ANCA IORDAN
Department of Electrical Engineering and Industrial Informatics
'Politehnica' University of Timisoara,
Revolutiei street, no. 5, Hunedoara,
ROMANIA
{raluca.rob, caius.panoiu, anca.iordan}@fih.upt.ro

Abstract: - Present paper studies the current harmonic spectrum generated by functioning of an electrothermal installation with electromagnetic induction. In order to analyze the electrical parameters that characterize the electrothermal installation functioning, measurement sets were accomplished using two methods. The first method consists in using a power and energy quality analyzer and the second method uses an acquisition system that contains an adapting interface and a data acquisition board connected to a computer. Paper contains also a simulation of the electrothermal installation functioning realized in PSCAD-EMTDC.

Key-Words: - nonlinear load, harmonic analysis, LabVIEW, PSCAD-EMTDC.

1 Introduction

The power quality problems are generated by many applications of static power electronic converters, fluorescent lamps, arc furnaces and so on. The frequency converters that are used in electrothermal installation sources lead to negative effects in the power distribution such as distortion of the current waveform, additional heating due to the rising of the current effective values [7], [8]. These problems can generate diminished quality in products or services, which lead to high costs for industrial and commercial activities. Nonlinear loads are responsible for the non sinusoidal regime generated into power distribution system. Analyzing the harmonic spectrum represents the first stage in designing the electronic devices that must compensate the distortion regime [15], [16], [17].

2. Description of harmonic analysis system

The electrothermal installation with electromagnetic induction that is studied in this paper is composed by an electronic converter CTC100K15 and a hardening inductor. The electric scheme of the electrothermal installation is presented in figure 1. The electrical characteristics are the followings: supplying voltage 3x400V, 50Hz, rated current 27A, control voltage 24Vdc, consumed power at high frequency 15kW. In order to study the harmonic distortion induced into the power system by the electrothermal installation, the current harmonic spectrum was analyzed using two methods [18], [19], [20], [21], [22], [23], [24], [25].

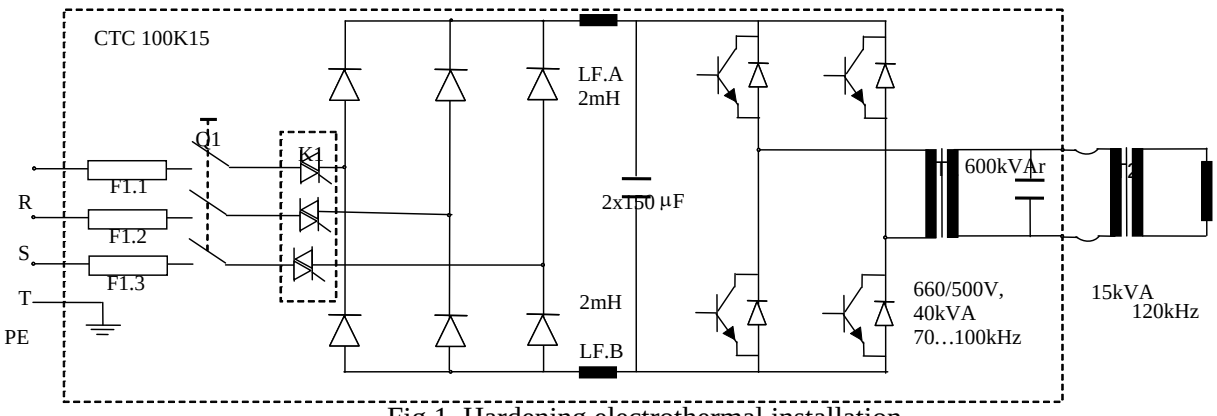

Fig.1. Hardening electrothermal installation.

2.1. Simulation using PSCAD-EMTDC

In the followings the simulation results using PSCAD-EMTDC program are presented. For simulating the power distribution a three phase voltage source
was chosen: U_n = 6kV, f = 50Hz. Power transformer has the following characteristics: U_{n1}/U_{n2} = 6 / 0,4kV, nominal power S_n = 400kVA.

The electric scheme presented in Fig. 2 contains a thyristor static contactor controlled by a pulse control block. PSCAD model for static contactor command is also shown in figure 2. The alternative voltage is rectified using a diode bridge rectified and a smoothing filter with L = 1mH, C = 300μF.

The inverter consists in four IGBT transistors and the model of inverter command is also presented in figure 2. High frequency transformer T1 has the following characteristics: U_1/U_2=0,6/0,5kV, S_{T1}=40kVA, f=100kHz and T2 has the following characteristics: U_1/U_2=0,5/0,1kV, S_{T2}=150kVA, f=100kHz. Inductor is modeled using a RL series circuit R=0,25Ω, L=1·10^{-7}H. The variation of current harmonics of 5, 7, 11 and 13 rank and also the total harmonic distortion (THD) variation are presented in figure 3. The values of these parameters are presented in table 1.

2.2. Current harmonic analysis using CA 8334B

The first method consists in using of a power and energy quality analyzer CA 8334B connected at the interface with the power distribution. Presented device is able to display in real time the electrical characteristics of the electric system that is connected to. As well, parameters in transient and permanent regime and also current and voltage harmonics can be computed [10], [11].

High frequency transformer which supplies the melting inductor, 150kVA, 70-120 kHz has the following transformation ratios: 3:1, 4:1, 5:1, 6:1, 7:1, 8:1, 9:1 and 10:1. The active power can be also adjusted.

In the followings the current harmonic spectrum for 5:1 transformation ratio are presented for the following situation: no-load operation, 4,5kW, 9kW and 15kW (figure 3).

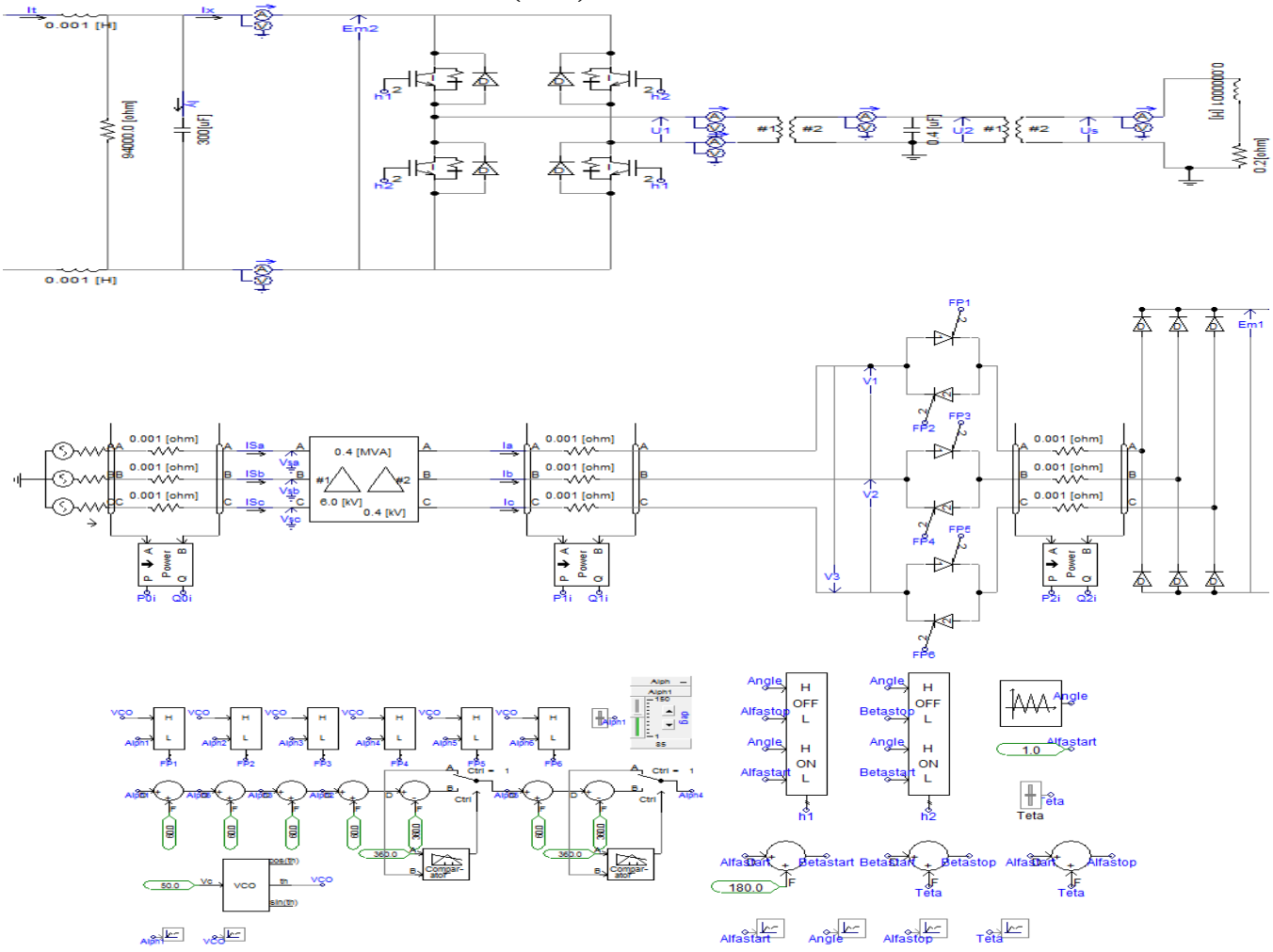

Fig. 2. Electrical scheme of the electrothermal installation (PSCAD-EMTDC simulation).

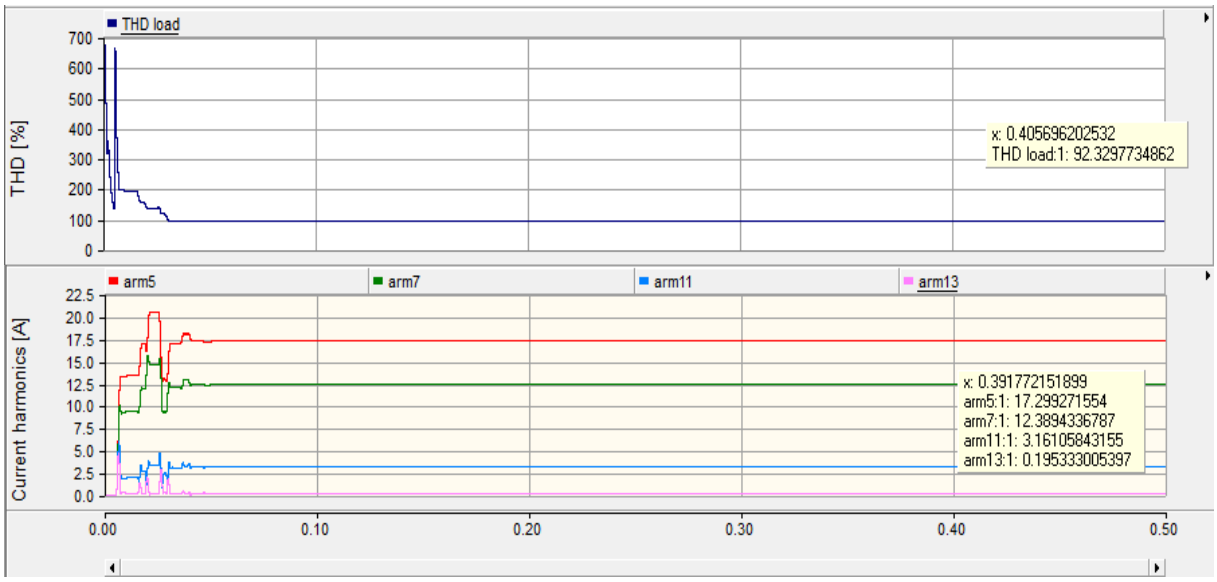

Fig. 3. Variation of current harmonics of 5, 7, 11 and 13 rank and THD (PSCAD simulation, P = 15kW).

Table 1. Values of current harmonics of 5, 7, 11 and 13 rank and THD.

Current harmonics and THD				
I_{arm5} [A]	I_{arm7} [A]	I_{arm11} [A]	I_{arm13} [A]	THD [%]
17,29	12,38	3,16	0,19	92,32

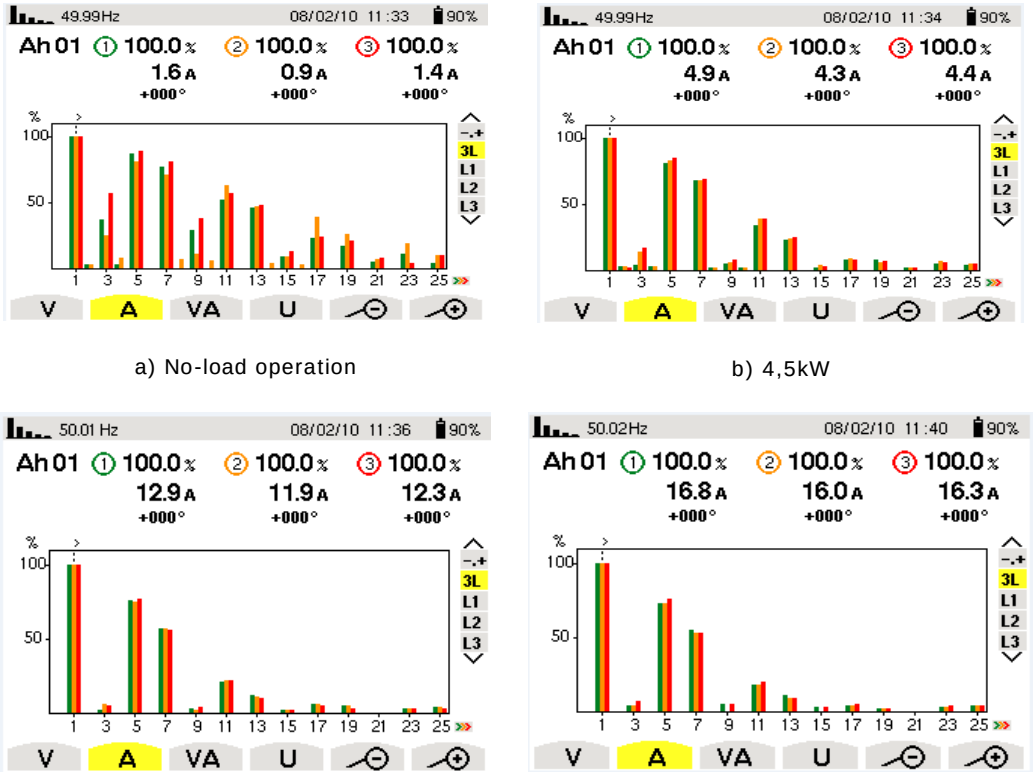

a) No-load operation b) 4,5kW

c) 9kW d) 15kW

Fig. 3. Current harmonic spectrum acquired with CA 8334B: a) No-load operation; b) P = 4,5kW; c) P = 9kW; d) P = 15kW, transformation ratio 5:1.

In table 2 the effective values of the current harmonics are presented (maximum rank is k = 25). The even rank harmonics and the multiple of 3 rank harmonics can be neglected. The effective value of the total current is given by the relation:

$$I_{total} = \sqrt{\sum_{k=1}^{25} I_k^2} \quad [A] \tag{1}$$

The harmonic distortion of the current curves THD_I is calculated with the following relation:

$$THD_I = \sqrt{\sum_{k=2}^{25} \frac{I_k}{I_1}^2} \quad 100 \quad [\%] \tag{2}$$

where k = 25 and represents the current harmonic rank [12], [13], [14].

2.3. Current harmonic analysis using the acquisition system

Harmonic spectrum analyzing was also accomplished using an acquisition system that contains an adapting interface and a data acquisition board connected to a computer [2], [3], [4]. The acquisition of voltage and current signals was made at the interface of the electrothermal installation with the power distribution.

The phase voltage uR(t), uS(t), uT(t), and phase currents iR(t), iS(t), iT(t) were acquired using the adapting interface which was designed in order to realise the galvanic isolation between the electrothermal installation and the acquisition system and also to accomplish the compatibility of voltage levels.

The data acquisition board has the following characteristics:

-16 analogic inputs, 250kS/s, 16 bit resolution;
-2 analogic outputs, 740ks/s, 16 bit resolution;
-24 TTL digital in/out;
-1 digital trigger;
-Windows 2000 (NT, XP), Linux compatibility.

The connection of the acquisition system is described in figure 4. In order to process the acquired data, two soft applications designed in LabVIEW 2011 were prepared: *acquisition application* and *computing application*. Using the *acquisition application*, the voltage and current samples are transformed into numeric data and stored into text documents.

This information is loaded by the *computing application* which is able to compute the most important electrical parameters that characterize the functioning of the electrothermal installation. In figure 5 the algorithm of the *computing application* is presented.

Table 2. Current harmonics (effective values) acquired with CA 8334B.

Rank	Current harmonics							
	No-load operation		P = 4.5kW		P = 9kW		P = 15kW	
	[%]	[A]	[%]	[A]	[%]	[A]	[%]	[A]
1	100	1.6	100	4.9	100	12.9	100	16.8
3	34	0.54	6	0.294	3.5	0.451	5	0.84
5	80	1.28	88.5	4.336	85.5	11.029	78	13.104
7	70.5	1.12	62	3.038	59.5	7.675	58.5	9.828
9	27	0.43	5	0.245	2.5	0.327	5	0.84
11	44.5	0.71	41.5	2.033	26.6	3.43	22.5	3.78
13	42.5	0.68	25	1.22	15	1.935	17.5	2.94
15	6.5	0.104	2.5	0.122	4	0.516	4	0.672
17	19.5	0.312	11.5	0.563	6	0.774	5	0.84
19	15.5	0.248	12	0.589	6	0.774	2.5	0.42
21	4	0.064	4	0.196	0	0	0	0
23	8	0.128	7.5	0.367	4	0.516	2.5	0.42
25	2.5	0.04	7.5	0.367	3.5	0.451	5	0.84
I_{total} [A]	2.667		7.669		19.098		24.022	
THD_I [%]	133.381		120.397		109.16		102.211	

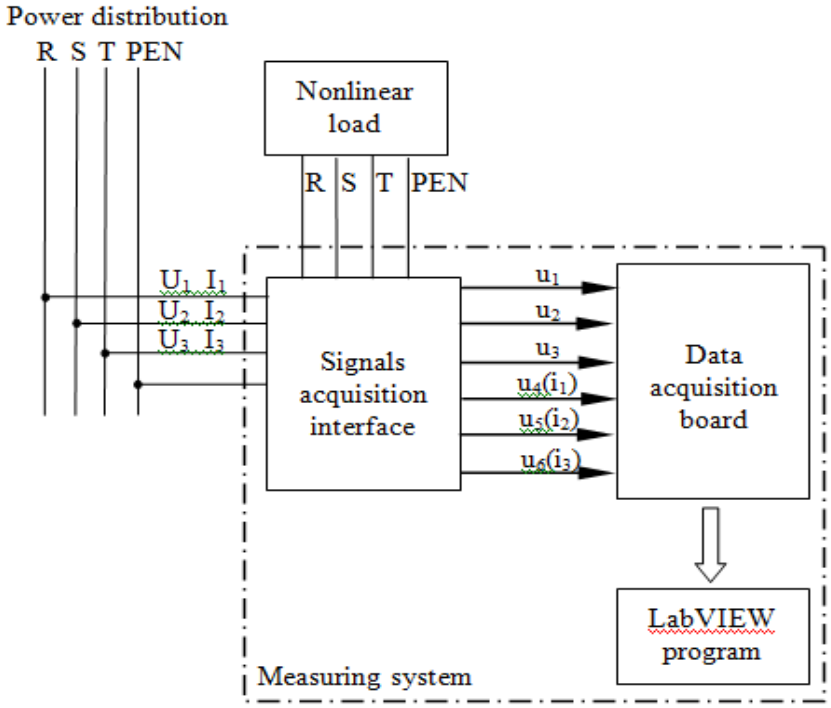

Fig. 4. Acquisition system connection.

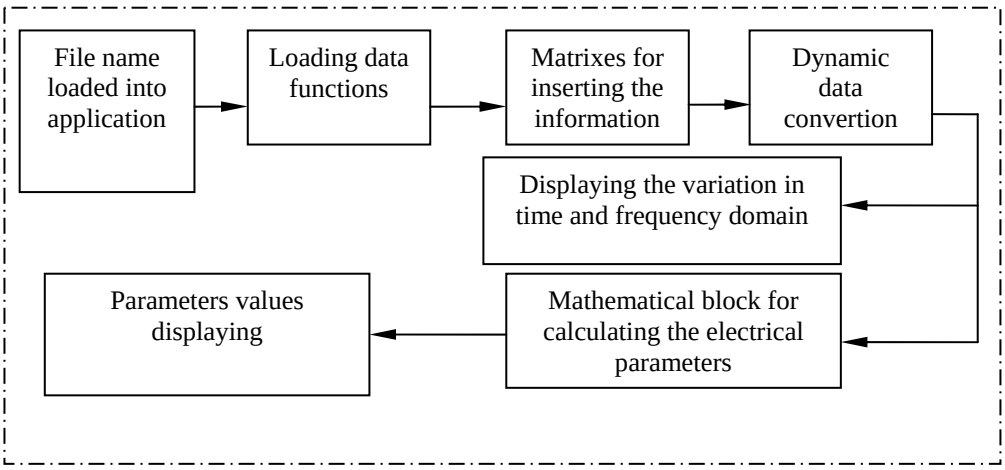

Fig. 5. *Computing application* block scheme.

In the followings the mathematical relation for computing the electrical parameters are presented.

The active power of *i* phase is computed with the relation:

$$P(i)=\sum_{k=1}^{50}U_{efk}(i)\cdot I_{efk}(i)\cdot\cos\Phi(i) \quad (3)$$

The reactive power of *i* phase is computed with the relation:

$$Q(i)=\sum_{k=1}^{50}U_{efk}(i)\cdot I_{efk}(i)\cdot\sin\Phi(i) \quad (4)$$

In relations (12) and (13). *k* represents the harmonic rank.

The harmonic voltage on *i* phase is computed as in the relation:

$$U_{thd}(i)=\frac{\sqrt{\sum_{n=2}^{50}U_{harm}(i,n)^2}}{U_{harm}(i,1)} \quad (5)$$

The harmonic current on *i* phase is computed as in the relation:

$$I_{thd}(i)=\frac{\sqrt{\sum_{n=2}^{50}I_{harm}(i,n)^2}}{I_{harm}(i,1)} \quad (6)$$

where *N* is the number of samples / period and *i* is the phase.

The total values of the active and reactive powers are computed as in the following relations:

$$P = \sum_{i=1}^{3} P_i \ . \ Q = \sum_{i=1}^{3} Q_i \quad (7)$$

The total apparent power is computed as:

$$S = 3 \cdot U_{ef} \cdot I_{ef} \quad (8)$$

The distorted power is computed as in the relation:

$$D = \sqrt{S^2 - P^2 - Q^2} \quad (9)$$

The total values of the harmonic voltages and currents are computed as in the followings:

$$U_{thd} = \sqrt{\frac{U_{thd(1)}^2 + U_{thd(2)}^2 + U_{thd(3)}^2}{3}} \quad (10)$$

$$I_{thd} = \sqrt{\frac{I_{thd(1)}^2 + I_{thd(2)}^2 + I_{thd(3)}^2}{3}} \quad (11)$$

In figure 6 the *3phase measuring system* subroutine is represented.

In figure 7 the scheme of measuring on each phase is depicted and the subroutine that computes the currents and voltage spectrum is presented in figure 8. The front panel of the application is presented in figure 9.

In figure 10 is presented the voltage and current harmonic spectrum that were recorded in the following conditions: active power adjusted at 4.5kW. 9kW and 15kW with transformation ratio 5:1. Table 3 synthesizes the current harmonic amplitudes that were generated with the acquisition system and table 4 shows the total harmonic distortion for the current curves computed by the acquisition system.

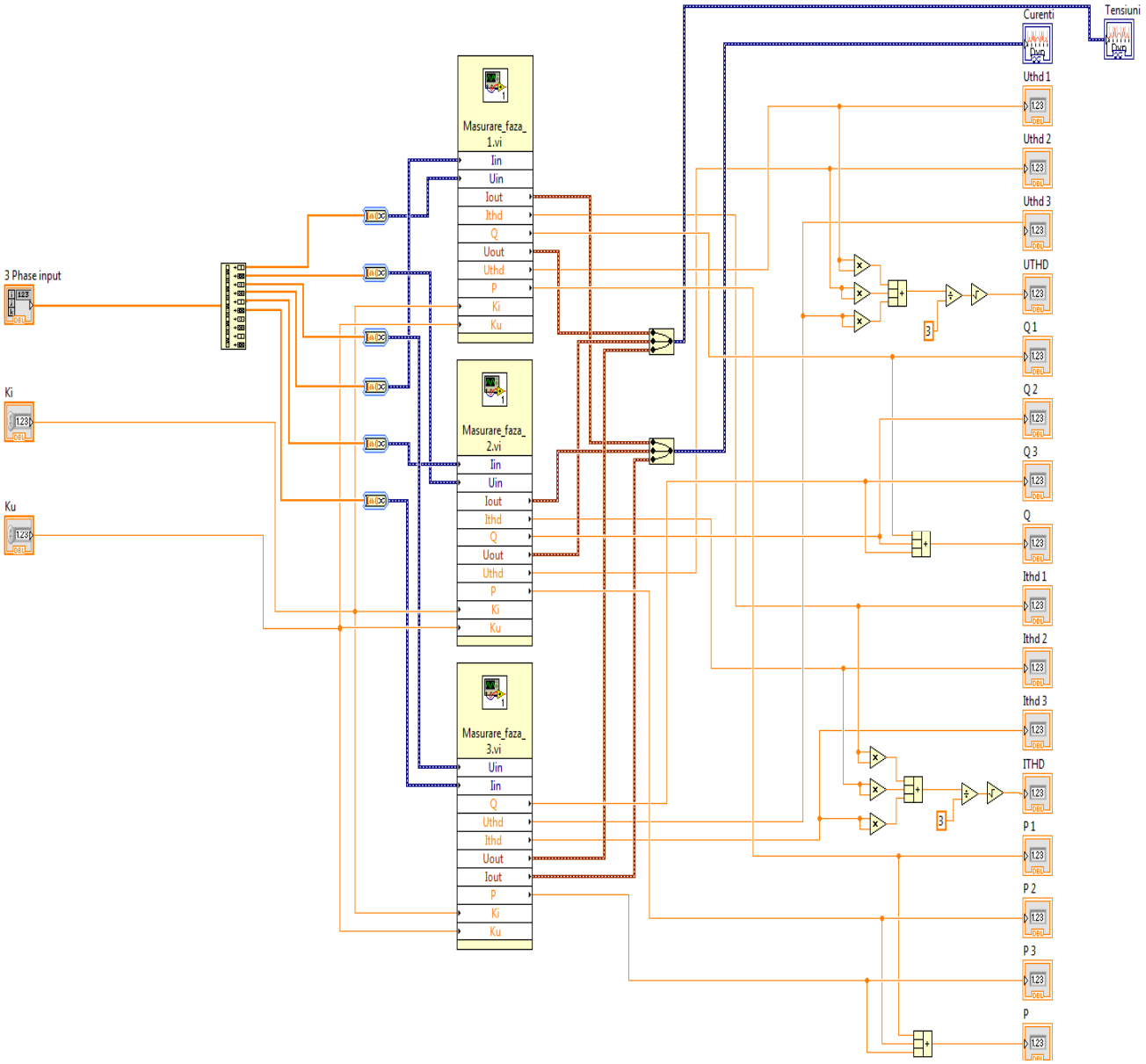

Fig. 6. *3phase measuring system* subroutine.

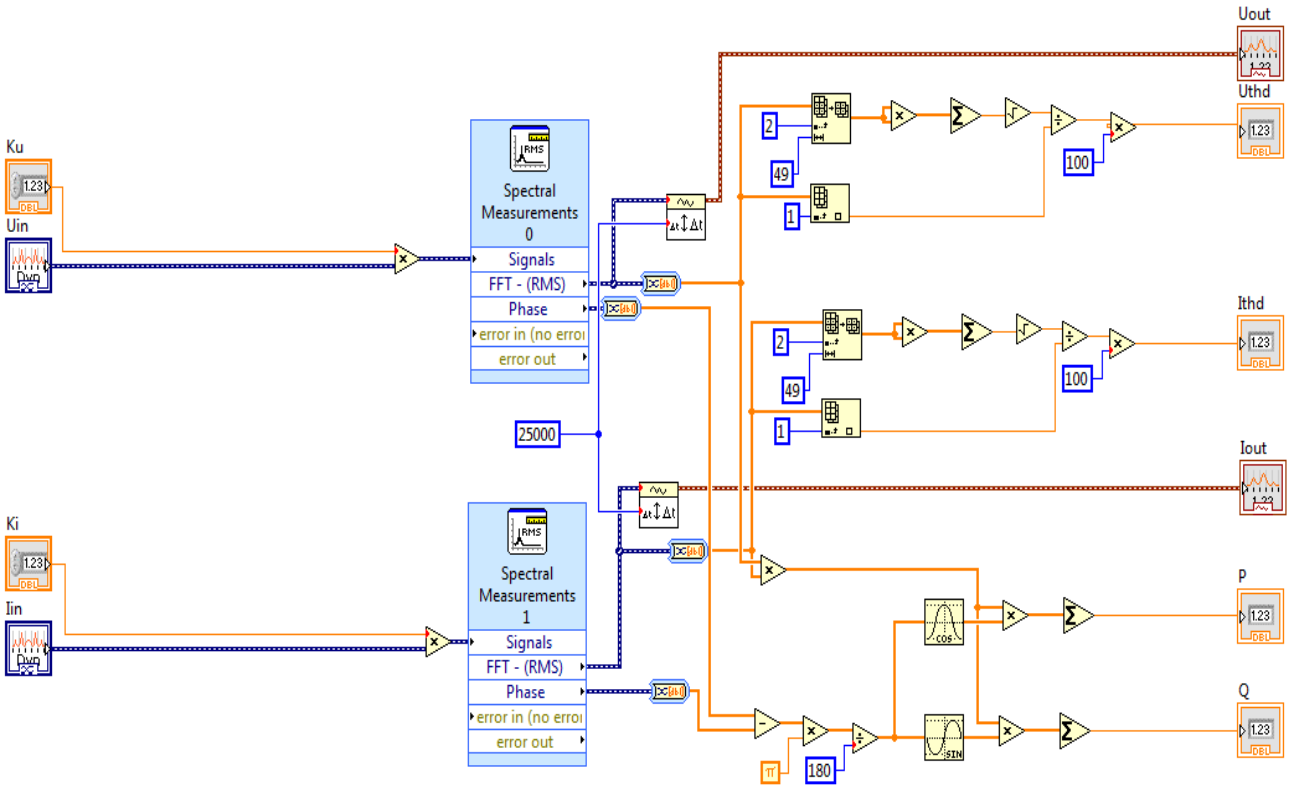

Fig. 7. LabVIEW code for measuring the electrical parameters on each phase.

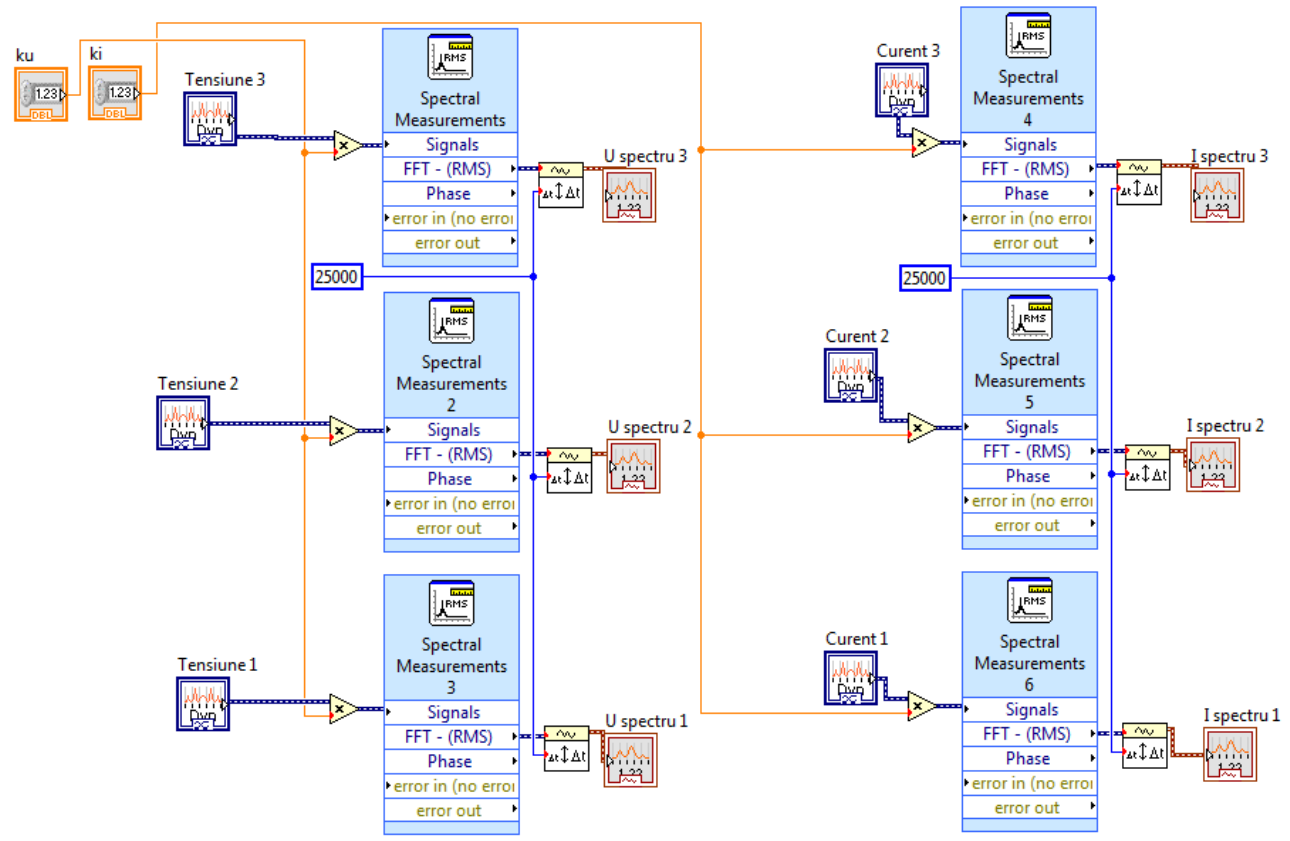

Fig. 8. LabVIEW code for computing the current and voltage spectrum.

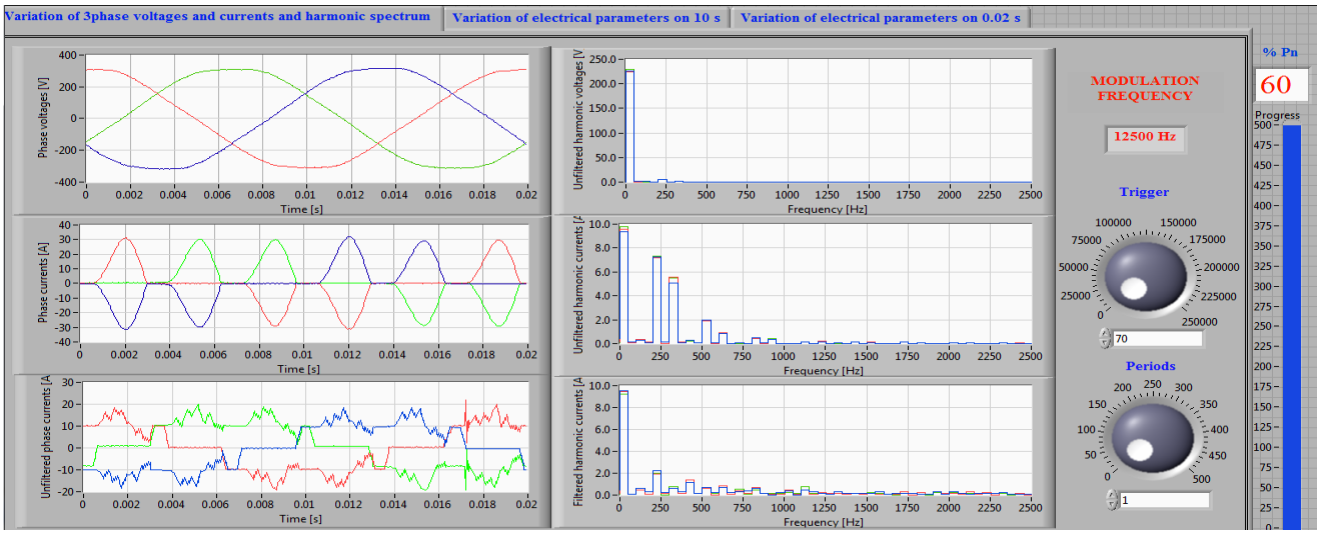

Fig. 9. Front panel of the application.

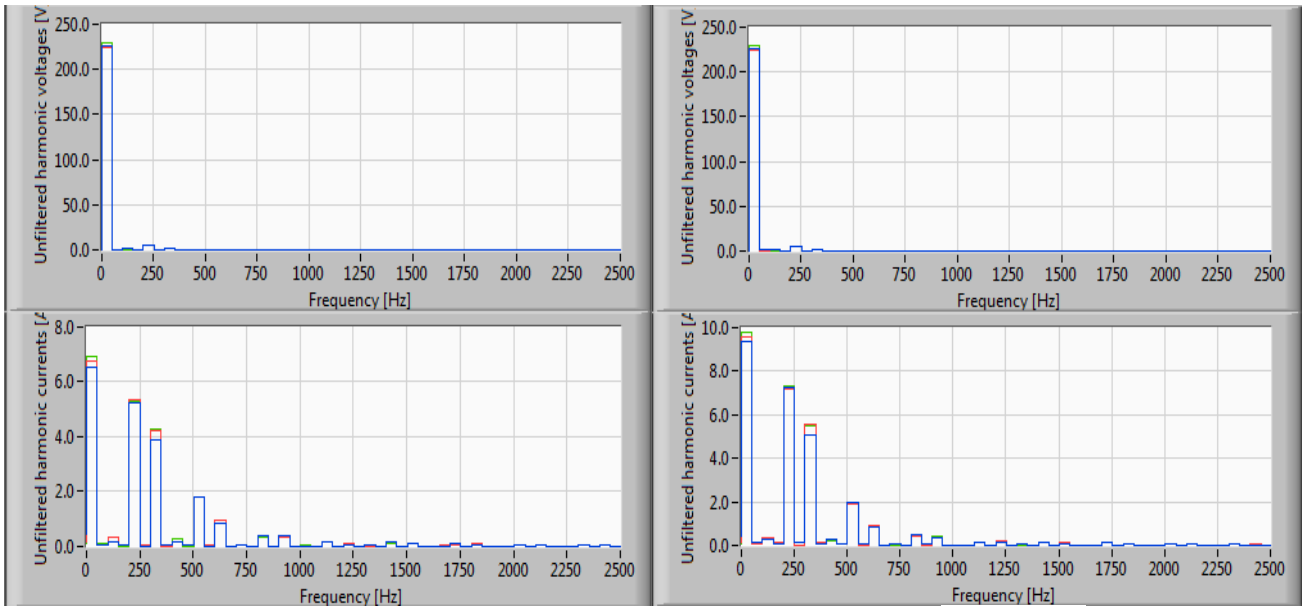

4.5kW 9kW

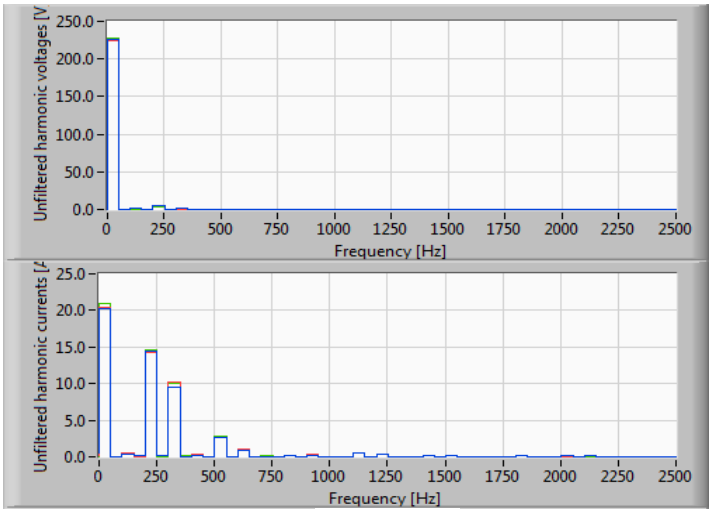

15kW

Fig. 10. Current and voltage harmonic spectrum generated with the acquisition system.

Table 3. Current harmonic amplitudes generated with the acquisition system.

	Harmonic currents [A]										
Active power [kW]	Rank										
	1	3	5	7	9	11	13	15	17	19	21
4.5	5	0.4	4	3.1	0.1	1.5	0.8	0.1	0.3	-	-
9	14	-	10	7	-	2	1	-	-	-	-
15	20	-	15	10	-	3	2	-	-	-	-

Table 4. Total harmonic distortion for the current curves generated with the acquisition system.

Computed parameter	Active power of the installation [kW]		
	4.5 (30% Pn)	9 (60% Pn)	15 (100% Pn)
THD for currents [%]	105.14	88.41	89.88

3. Conclusions

Harmonic analyzing is very necessary for designing the electronic devices which must compensate the distorted regime introduced into the power system by the nonlinear loads. This paper proposes three different and accessible methods for following the variation in time and frequency domain of the most important electric parameters that characterize the functioning of an electrothermal installation with electromagnetic induction.

Using PSCAD-EMTDC simulations of the electric equipments functioning can be accomplished. So, the command and control elements for the electrothermal installation were modeled. The PSCAD EMTDC is able to display the variation of the 5^{th}, 7^{th}, 11^{th} and 13^{th} current harmonics.

Acquisition with CA8334B power analyzer represents a very practical method for studying in real time of the electrical parameters variation. As well, this method generates the variation of current and voltage harmonics when the electrothermal installation is functioning at 4.5kW, 9kW and 15kW. From Table 2 can be concluded that the total harmonic distortion for phase currents reaches high values that step over 133%.

Data acquisition system which is described in the third method presents the advantage of permanently improvement concerning the soft applications that compute in real time the electrical parameters. The present method follows the variation of the phase current spectrum when the electrothermal installation is functioning at 4.5kW, 9kW and 15kW.

Modeling and simulation are essential tools in many areas of science and engineering, for example in Netlogo language [9].

Using both data acquisition methods, the variation of the current harmonics are displayed.

The nonlinear load described in this paper represents a current harmonics source. Following the results, the distortion of the current curves falls below the standard limits and the current harmonics must be compensated using appropriate devices [1], [5], [6].

References

[1] Akagi. A., Watanabe. E., Aredes. M.: The P-Q theory for active filter control: some problems and solutions. *Revista Controle & Automacao /* Vol.15, no.1, March 2004.

[2] Doroshin, A. V., Neri, F. (2014) Open research issues on Nonlinear Dynamics, Dynamical Systems and Processes. WSEAS Transactions on Systems, 13, in press.

[3] Rob Raluca. Sora Ioan. Panoiu Caius. Panoiu Manuela. Using Active Filters in Reducing of the Total Harmonic Distortion on Electro Thermal Installation with Electromagnetic Induction. *International Symposium of Power Electronics. Electrical Drives. Automation and Motion. SPEEDAM 2010*, Pisa, Italy, pp. 233-238.

[4] Panoiu Caius, Rob Raluca, Manuela Panoiu, Gabriel Popa, Measurements of the Electrical

Parameters of an Electro Thermal Installation with Electromagnetic Induction. *Proceedings of the 14th WSEAS International Conference on System.* 2010, Corfu, Greece, pp. 216-221.

[5] G.O Tirian, C.Pinca-Bretotean, D.Cristea, M. Topor Research on the elimination of cracks in continuous casting plant using fuzzy logic, *Proceedings of the 8th WSEAS Int. Conf.on CIRCUITS, SYSTEMS, ELECTRONICS, CONTROL & SIGNAL PROCESSING (CSECS '09),* Puerto De La Cruz, Tenerife, Canary Islands, Spain, December 14-16, pp.273-278.

[6] Jacobina. C.; de Rossiter Correa. M.; Ferreira Pinheiro. R.; de Silva. E.; Nogueira Lima. A., Modeling and control of unbalanced three phase systems containing PWM converters. *IEEE Transactions on Industry Applications.* no. 6, vol. 37, pp. 1807-1816.

[7] Kapoor A.K., Mahanty R., A quasi passive filter for power quality improvement, *Proceedings of IEEE International Conference of Industrial Technology* vol.1, 2000, pp. 526-529.

[8] Zamora. I.., A. J. Mazon, P. Eguia, I. Albizu. K., J. Sagastabeitia, E. Fernández, Simulation by MATLAB/Simulink of active filters for reducing THD created by industrial systems. *IEEE Bologna Power Tech. Conference*, 23-26 June 2003, Bologna, Italy.

[9] Ionel Muscalagiu, Cosmina Illes, Horia Emil Popa, Large Scale Multi-Agent-Based Simulation using NetLogo for the multi-robot exploration problem, *IEEE 11th International Conference on Industrial Informatics* 2013, Bochum, Germany, pag. 225-230.

[10] Chauvin Arnoux, Three phase power quality analyzer CA 8332B, CA 8334B. User's manual.

[11] Ioan Baciu, Cuntan Corina, Manuela Panoiu, Cristian Abrudean, Highlighting the existing harmonics on locomotives with dc motors, 13th WSEAS International Conference on Electric Power Systems, High Voltages, Electric Machines, 2013.

[12] Ciufudean, C., Neri, F. (2014) Open research issues on Multi-Models for Complex Technological Systems. WSEAS Transactions on Systems, 13, in press.

[13] Neri, F. (2014) Open research issues on Computational Techniques for Financial Applications. WSEAS Transactions on Systems, 13, in press.

[14] Karthikeyan, P., Neri, F. (2014) Open research issues on Deregulated Electricity Market: Investigation and Solution Methodologies. WSEAS Transactions on Systems, 13, in press.

[15] Panoiu, M., Neri, F. (2014) Open research issues on Modeling, Simulation and Optimization in Electrical Systems. WSEAS Transactions on Systems, 13, in press.

[16] Neri, F. (2014) Open research issues on Advanced Control Methods: Theory and Application. WSEAS Transactions on Systems, 13, in press.

[17] Hájek, P., Neri, F. (2013) An introduction to the special issue on computational techniques for trading systems, time series forecasting, stock market modeling, financial assets modeling WSEAS Transactions on Business and Economics, 10 (4), pp. 201-292.

[18] Azzouzi, M., Neri, F. (2013) An introduction to the special issue on advanced control of energy systems (2013) WSEAS Transactions on Power Systems, 8 (3), p. 103.

[19] Bojkovic, Z., Neri, F.(2013) An introduction to the special issue on advances on interactive multimedia systems WSEAS Transactions on Systems, 12 (7), pp. 337-338.

[20] Pekar(, L., Neri, F. (2013) An introduction to the special issue on advanced control methods: Theory and application (2013) WSEAS Transactions on Systems, 12 (6), pp. 301-303.

[21] Guarnaccia, C., Neri, F. (2013) An introduction to the special issue on recent methods on physical polluting agents and environment modeling and simulation WSEAS Transactions on Systems, 12 (2), pp. 53-54.

[22] Neri, F. (2012) An introduction to the special issue on computational techniques for trading systems, time series forecasting, stock market modeling, and financial assets modeling WSEAS Transactions on Systems, 11 (12), pp. 659-660.

[23] Muntean, M., Neri, F. (2012) Foreword to the special issue on collaborative systems WSEAS Transactions on Systems, 11 (11), p. 617.

[24] Pekar(, L., Neri, F. (2012) An introduction to the special issue on time delay systems: Modelling, identification, stability, control and applications WSEAS Transactions on Systems, 11 (10), pp. 539-540.

[25] Volos, C., Neri, F. (2012) An introduction to the special issue: Recent advances in defense systems: Applications, methodology, technology WSEAS Transactions on Systems, 11 (9), pp. 477-478.

Stability Enhancement of Multimachine Power System via New Coordinated Design of PSSs and SVC

Ali, E. S.[a] and. Abd-Elazim, S. M[b]
a- Electric Power and Machine Department, Faculty of Engineering, Zagazig University, Zagazig, Egypt,
E-mail address: : ehabsalimalisalama@yahoo.com
b- Electric Power and Machine Department, Faculty of Engineering, Zagazig University, Zagazig, Egypt,
E-mail address: sahareldeep@yahoo.com

Abstract- In this paper, the assessment of new coordinated design of Power System Stabilizers (PSSs) and Static Var Compensator (SVC) in a multimachine power system via statistical method is proposed. The coordinated design problem of PSSs and SVC over a wide range of loading conditions is handled as an optimization problem. The Bacterial Swarming Optimization (BSO), which synergistically couples the Bacterial Foraging (BF) with the Particle Swarm Optimization (PSO), is employed to seek for optimal controllers parameters. By minimizing the proposed objective function, in which the speed deviations between generators are involved; stability performance of the system is enhanced. To compare the capability of PSS and SVC, both are designed independently, and then in a coordinated manner. Simultaneous tuning of the BSO based coordinated controller gives robust damping performance over wide range of operating conditions and large disturbance in compare to optimized PSS controller based on BSO (BSOPSS) and optimized SVC controller based on BSO (BSOSVC). Moreover, a statistical T test is executed to validate the robustness of coordinated controller versus uncoordinated one.

Key-Words: SVC; PSSs; Multimachine Power System; Coordinated design; Bacteria Swarm Optimization; Statistical Assessment.

1. Introduction

The power transfer in an integrated power system is forced by transient stability, voltage stability and small signal stability. These factors limit a full utilization of available transmission corridors. Flexible AC Transmission System (FACTS) is the technology that supplies the needed corrections of the transmission functionality in order to use the existing transmission facilities and hence, reducing the gap between the stability limit and thermal limit [1].

Recently, there has been a surge of interest in the use and development of FACTS controllers in power transmission systems [2-6]. These controllers utilize power electronics devices to provide more flexibility to AC power systems. The most popular type of FACTS devices in terms of application is the SVC. This device is well known to improve power system properties such as steady state stability limits, voltage regulation and var compensation, dynamic over voltage and under voltage control, and mitigate power system oscillations. The SVC is an electronic generator that dynamically controls the flow of power through a variable reactive admittance to the transmission network.

In last few years, many researchers have introduced techniques for designing SVC to improve the damping of electromechanical oscillations of power systems and enhance power systems stability. A robust control theory in designing SVC controller to damp out power system swing modes is discussed in [7]. An adaptive network based fuzzy inference system (ANFIS) for SVC is illustrated in [8] to alleviate the damping of power systems. A multi input, single output fuzzy neural network is developed in [9] for voltage stability evaluation of the power systems with SVC. A method of determining the location of a SVC to enhance the stability of power system is suggested in [10]. A systematic approach for designing SVC controller, based on wide area signals, to increase the damping of power system oscillations is introduced in [11]. Genetic Algorithm (GA) optimization technique is employed for the simultaneous tuning of a PSS and a SVC based controller in [12]. A state estimation problem of power systems incorporating various FACTS devices is addressed in [13]. A novel hybrid method for simulation of power systems equipped with SVC is suggested in [14]. The design of SVC with delayed input signal using a state space model based on Pade approximation method is presented in [15]. A new optimization algorithm known as Bacterial Foraging (BF) for designing SVC to damp power system electromechanical oscillations for single machine infinite bus system and multimachine system are introduced in [16-17]. An application of probabilistic theory to the coordinated design of PSSs and SVC is employed in [18]. The application

of the decentralized modal control method for pole placement in multimachine power system utilizing FACTS devices is developed in [19]. The parameter tuning of a PID controller for a FACTS based stabilizer employing multi-objective evolutionary algorithm is illustrated in [20]. A comprehensive assessment of the effects of the PSS and FACT device when applied independently and also through coordinated application is carried out in [21]. other works related to dynamical systems, computational techniques, collaborative systems, time delay systems, recent methods on physical polluting agents and environment modelling and simulation, interactive multimedia systems, on advanced control of energy systems, defence systems, modelling, simulation and optimization in electrical systems are given in [22-36].

Different optimization techniques have been adopted to solve a variety of engineering problems in the past decade. GA has attracted the attention in the field of controller parameter optimization. Although GA is very satisfactory in finding global or near global optimal result of the problem; it needs a very long run time that may be several minutes or even several hours depending on the size of the system under study. Moreover swarming strategies in bird flocking and fish schooling are used in the PSO and introduced in [37]. However, PSO suffers from the partial optimism, which causes the less exact at the regulation of its speed and the direction. Also, the algorithm cannot work out the problems of scattering and optimization [38-41]. In addition, the algorithm pains from slow convergence in refined search stage, weak local search ability and algorithm may lead to possible entrapment in local minimum solutions. A relatively newer evolutionary computation algorithm, called BF scheme has been addressed by [42-44] and further established recently by [45-52]. The BF algorithm depends on random search directions which may lead to delay in reaching the global solution. A new algorithm BF oriented by PSO is developed that combine the above mentioned optimization algorithms [53-54]. This combination aims to make use of PSO ability to exchange social information and BF ability in finding a new solution by elimination and dispersal. This new hybrid algorithm called Bacterial Swarm Optimization (BSO) is adopted in this paper to solve the above mentioned problems and drawbacks.

In this paper, a comprehensive assessment of the effects of the PSSs and SVC based control when applied independently and also through coordinated application has been carried out. The design problem of PSS and SVC based controller to improve power system stability is transformed into an optimization problem. The design objective is to improve the stability of a multimachine power system, subjected to a disturbance. BSO technique is employed to search for the optimal PSS and SVC controller parameters. BSO based SVC controller (BSOSVC) and BSO based PSS (BSOPSS) are presented and their performances are compared with the coordinated design of BSOPSS and BSOSVC. Simulation results are presented to demonstrate the effectiveness of the proposed controller to improve the power system dynamic stability. Furthermore, a statistical T test is performed to prove the robustness of coordinated controller versus uncoordinated one.

2. Problem Statement

A. Power System Model

A power system can be modelled by a set of nonlinear differential equations as:

$$\dot{X} = f(X,U) \quad (1)$$

Where X is the vector of the state variables and U is the vector of input variables. In this study $X = [\delta, \omega, E'_q, E_{fd}, V_f]^T$ and U is the PSS and SVC output signals. Here, δ and ω are the rotor angle and speed, respectively. Also, E'_q, E_{fd} and V_f are the internal, the field, and excitation voltages respectively.

In the design of PSS and SVC, the linearized incremental models around an equilibrium point are usually employed. Therefore, the state equation of a power system with n machines and m PSS and SVC can be written as:

$$\dot{X} = AX + Bu \quad (2)$$

Where A is a $5n \times 5n$ matrix and equals $\partial f / \partial X$ while B is a $5n \times m$ matrix and equals $\partial f / \partial U$.

Both A and B are evaluated at a certain operating point. X is a $5n \times 1$ state vector and U is an $m \times 1$ input vector.

B. PSS Modelling and Damping Controller Design

The operating function of a PSS is to produce a proper torque on the rotor of the machine involved in such a way that the phase lag between the exciter input and the machine electrical torque is compensated. The supplementary stabilizing signal considered is one proportional to speed. A widely speed based used conventional PSS is considered

throughout the study [55]. The block diagram of the i^{th} PSS with excitation system is shown in Fig. 1. Where $\Delta\omega_i$ is the deviation in speed from the synchronous speed. This type of stabilizer consists of a washout filter, a dynamic compensator. The output signal is fed as a supplementary input signal, U_i to the regulator of the excitation system. The washout filter, which essentially is a high pass filter, is used to reset the steady state offset in the output of the PSS. The value of the time constant T_W is usually not critical and it can range from 0.5 to 20 s. The dynamic compensator is made up to two lead lag circuits and an additional gain. The adjustable PSS parameters are the gain of the PSS, K_i and the time constants, $T_{1i}-T_{4i}$. The lead lag block present in the system provides phase lead compensation for the phase lag that is introduced in the circuit between the exciter input and the electrical torque. The required phase lead can be derived from the lead lag circuit even if the denominator portion consisting of T_{2i} and T_{4i} gives a fixed lag angle [56].

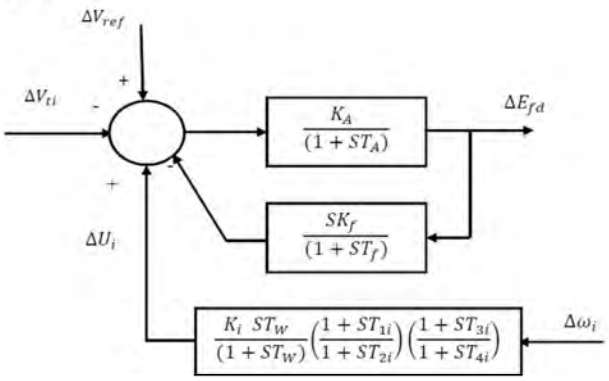

Fig. 1. Block diagram of i^{th} PSS with excitation system.

C. SVC Modelling and Damping Controller Design

The thyristor controlled reactor (TCR) in parallel with a fixed capacitor bank shown in Fig. 2, is used in this paper to develop the desired SVC model. The system is then shunt connected to the AC system through a set up transformer to bring the voltages up to the required transmission levels [8].

It is obvious from (3) and Fig. 3, if the firing angle α of the thyristors is controlled; SVC is able to control the bus voltage magnitude. Time constant (T_r) and gain (K_r) represent the thyristors firing control system. The SVC parameters are given in Appendix.

$$\dot{B}_e = \frac{1}{T_r}\left[-B_e + K_r(V_{ref} - V_t + V_s)\right] \quad (3)$$

The variable effective susceptance of the TCR is given by

$$B_V = -\frac{(2\pi - 2\alpha + \sin 2\alpha)}{\pi X_L} \quad \pi/2 \le \alpha \le \pi \quad (4)$$

Where X_L is the reactance of the fixed inductor of SVC. The effective reactance is

$$X_e = X_C \frac{\pi / r_x}{\sin 2\alpha - 2\alpha + \pi(2 - 1/r_x)} \quad (5)$$

Where X_e=-1/B_e and $r_x = X_e / X_L$.

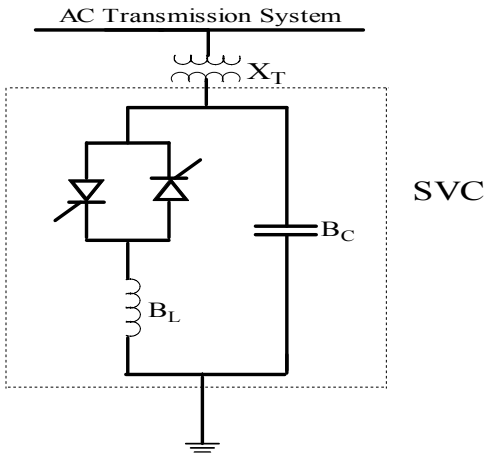

Fig. 2. SVC equivalent circuit.

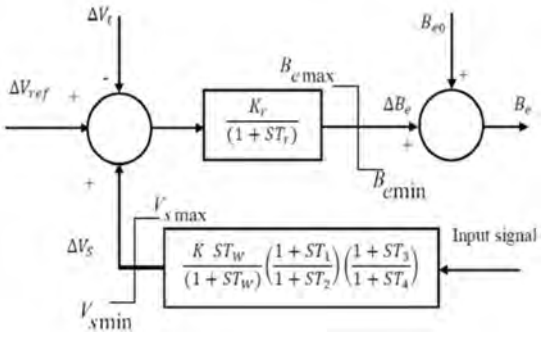

Fig. 3. Block diagram of SVC.

An auxiliary stabilizing signal from speed can be imposed on the SVC control loop. The block diagram of a SVC with auxiliary stabilizing signal is shown in Fig. 3. This controller may be considered as a lead lag compensator. It comprises gain block, limiter, signal washout block and two stages of lead lag compensator. The parameters of the damping controllers for the purpose of simultaneous coordinated design are obtained using the BSO algorithm.

D. System under Study and SVC Position

Fig. 4 shows the single line diagram of the test system used. Details of system data are given in [57]. The participation matrix can be used in mode identification. Table (1) shows the eigenvalues, and frequencies associated with the rotor oscillation modes of the system. Examining Table (1) shows that the 0.2371 Hz mode is the interarea mode with G1 swinging against G2 and G3. The 1.2955 Hz mode is the intermachine oscillation local to G2. Also, the 1.8493 Hz mode is the intermachine mode local to G3. The positive real part of eigenvalue of G1 indicates instability of the system. The system and generator loading levels are given in Table (2).

In order to determine the suitable position of the SVC in the system, two strategies will be shown below. The first one is based on studying the effect of load percentage while the second is concerned with the line outage on system voltages [58]. Tables (3 and 4) show the effect of load percentage and line outage on bus voltages of the system. It can be noticed that the voltages are affected significantly at buses numbered 5 and 6, respectively which are load buses. The reasons that cause the significant voltage change are the connection of these buses with the longest lines in the system which has greater resistances and reactances than the others. Consequently, the choice of buses number 5 or 6 for placing the SVC controller is expected to be the more suitable choice. Because both of them are close to machine number 1 which causes the system instability due to its unstable mechanical mode. Moreover, bus number 5 is the worst one and will be considered in this paper as the best position for installing the SVC controller.

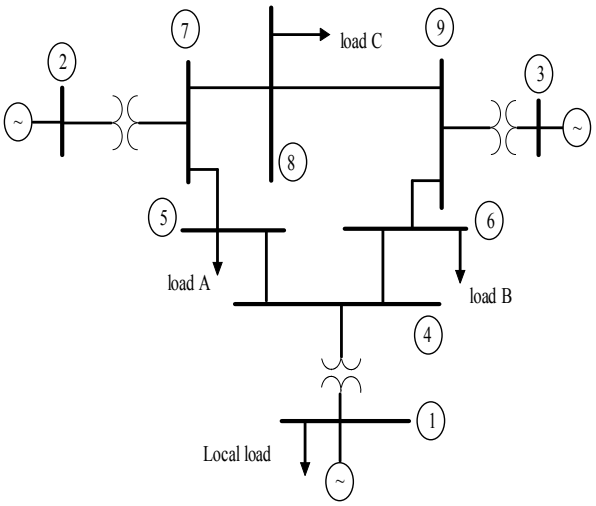

Fig. 4. System under study.

Table (1) The eigenvalues, and frequencies of the rotor oscillation modes of the system.

Generator	Eigenvalues	Frequencies	Damping ratio ζ
G1	**+0.15 ± 1.49j**	0.2371	**-0.1002**
G2	-0.35 ± 8.14j	1.2295	0.0430
G3	-0.67 ± 11.62j	1.8493	0.0576

Table (2) Loading of the system (in p.u).

	Light		Normal case		Heavy	
Generator	P	Q	P	Q	P	Q
G1	0.965	0.22	1.716	0.6205	3.57	1.81
G2	1.0	-0.193	1.63	0.0665	2.2	0.713
G3	0.45	-.267	0.85	-1086	1.35	0.43
Load	P	Q	P	Q	P	Q
A	0.7	0.35	1.25	0.5	2.0	0.9
B	0.5	0.3	0.9	0.3	1.8	0.6
C	0.6	0.2	1.00	0.35	1.6	0.65
at G1	0.6	0.2	1.00	0.35	1.6	0.65

Table (3) Effect of load percentage on load bus voltages.

% Load	**0.25**	**0.50**	**0.75**	**1.00**	**1.25**	**1.50**	**1.75**
Bus 4	1.06	1.05	1.04	1.03	1.01	0.99	0.98
Bus 5	1.06	1.04	1.02	0.99	0.96	**0.94**	**0.90**
Bus 6	1.06	1.05	1.03	1.01	0.99	0.97	**0.94**
Bus 7	1.05	1.04	1.04	1.03	1.01	1.00	0.98
Bus 8	1.05	1.04	1.03	1.02	0.99	0.98	0.96
Bus 9	1.05	1.05	1.04	1.03	1.02	1.01	1.00

Table (4) Effect of line outage on load bus voltages.

line	**4-5**	**4-6**	**5-7**	**6-9**	**7-8**	**8-9**
Bus 4	1.039	1.028	0.996	1.005	1.016	1.022
Bus 5	**0.839**	0.998	**0.938**	0.968	0.974	0.989
Bus 6	1.020	**0.942**	0.975	0.964	0.999	1.009
Bus 7	0.988	1.022	1.017	1.016	1.019	1.010
Bus 8	0.989	1.006	1.001	1.005	0.969	0.978
Bus 9	1.024	1.017	1.019	1.023	1.013	1.034

3. Objective function

The parameters of the PSSs and SVC may be elected to reduce the following objective function:

$$J = \int_0^{\infty} t\left(\left|\Delta w_{12}\right| + \left|\Delta w_{23}\right| + \left|\Delta w_{13}\right|\right)dt \qquad (6)$$

Where $\Delta w_{12} = \Delta w_1 - \Delta w_2$, $\Delta w_{23} = \Delta w_2 - \Delta w_3$, and $\Delta w_{13} = \Delta w_1 - \Delta w_3$.

This index is based on the Integral of Time multiple Absolute Error (ITAE). The merit of this selected performance index is that minimal dynamic plant information is needed. To reduce the computational burden, the value of the wash out time constant T_W is fixed to 10 second, the values of T_{2i} and T_{4i} are kept constant at a reasonable value of 0.05 second and tuning of T_{1i} and T_{3i} are undertaken to reach the net phase lead required by

the system. Based on the objective function J optimization problem can be stated as: Minimize J subjected to:

$$K_i^{\min} \le K_i \le K_i^{max}$$
$$T_{1i}^{\min} \le T_{1i} \le T_{1i}^{max}$$
$$T_{3i}^{\min} \le T_{3i} \le T_{3i}^{max} \quad (7)$$

Typical ranges of the optimized parameters are [1-100] for K_i and [0.06-1.0] for T_{1i} and T_{3i}.

This paper focuses on coordinated design of PSSs and SVC via BSO algorithm. The object of the optimization is to search for the optimum controller parameters setting that improve the damping characteristics of the system. Moreover, all controllers are designed simultaneously, taking into consideration the interaction among them.

4. Hybrid BF-PSO Optimization Algorithm

PSO is a stochastic optimization technique that draws inspiration from the behaviour of a flock of birds or the collective intelligence of a group of social insects with limited individual capabilities. In PSO a population of particles is initialized with random positions $\vec{X}_i$ and velocities $\vec{V}_i$, and a fitness function using the particle's positional coordinates as input values. Positions and velocities are adjusted, and the function is evaluated with the new coordinates at each time step [37-38]. The velocity and position update equations for the d-th dimension of the i-th particle in the swarm may be given as follows:

$$V_{id}(t+1) = \omega.V_{id}(t) + C_1.\varphi_1.(X_{lid} - X_{id}(t)) + C_2.\varphi_2.(X_{gd} - X_{id}(t)) \quad (8)$$

$$X_{id}(t+1) = X_{id}(t) + V_{id}(t+1) \quad (9)$$

Where X_{lid} is the best position of each bacterial and X_{gd} is the global best bacterial.

On the other hand, the BF is based upon search and optimal foraging decision making capabilities of the Escherichia coli bacteria [53]. The coordinates of a bacterium here represent an individual solution of the optimization problem. Such a set of trial solutions converges towards the optimal solution following the foraging group dynamics of the bacteria population. Chemotactic movement is continued until a bacterium goes in the direction of positive nutrient gradient. After a certain number of complete swims the best half of the population undergoes reproduction, eliminating the rest of the population. In order to escape local optima, an elimination dispersion event is carried out where, some bacteria are liquidated at random with a very small probability and the new replacements are initialized at random locations of the search space. A detailed description of the complete algorithm can be traced in [53-54]. Also, the flow chart of BSO is shown in Fig. 5.

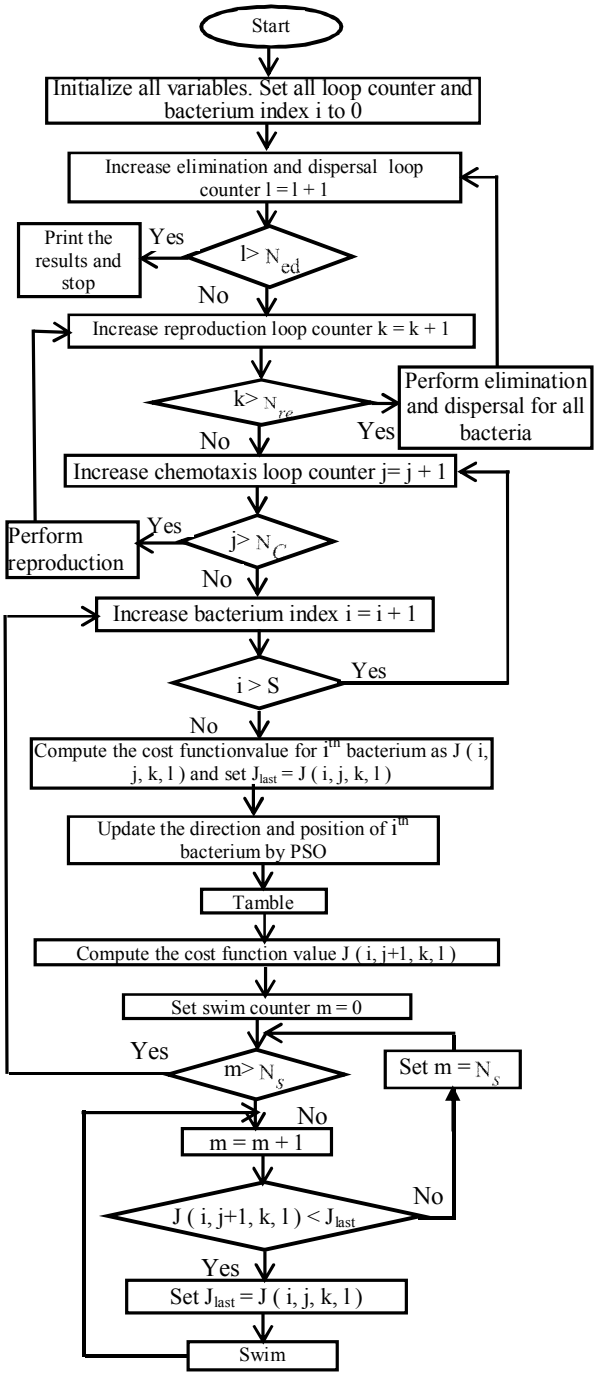

Fig. 5. Flow chart of BSO algorithm.

[Step 1] Initialize parameters n, S, N_C, N_S, N_{re}, N_{ed}, P_{ed}, $C(i)(i=1,2,.....,N)$, ϕ^i.

Where,

n: Dimension of the search space,

S: The number of bacteria in population,

N_{re}: The number of reproduction steps,

N_C: The number of chemotactic steps,

N_S: Swimming length after which tumbling of bacteria is performed in a chemotaxis loop,

N_{ed}: The number of elimination-dispersal events to be imposed over the bacteria,

P_{ed}: The probability with which the elimination and dispersal will continue,

$C(i)$: The size of the step taken in the random direction specified by the tumble,

ω: The inertia weight,

C_1, C_2: The swarm confidence,

$\vec{\theta}(i,j,k)$: Position vector of the i-th bacterium, in j-th chemotactic step and k-th reproduction,

$\vec{V}_i$: Velocity vector of the i-th bacterium.

[Step 2] Update the following

$J(i,j,k)$: Cost or fitness value of the i-th bacterium in the j-th chemotaxis, and the k-th reproduction loop.

$\vec{\theta}_{g\_best}$: Position vector of the best position found by all bacteria.

$J_{best}(i,j,k)$: Fitness value of the best position found so far.

[Step 3] Reproduction loop: $k = k+1$

[Step 4] Chemotaxis loop: $j = j+1$

[Sub step a] For i=1, 2,…, S, take a chemotaxis step for bacterium i as follows.

[Sub step b] Compute fitness function, $J(i,j,k)$.

[Sub step c] Let $J_{last} = J(i,j,k)$ to save this value since one may find a better cost via a run.

[Sub step d] Tumble: generate a random vector $\Delta(i) \in R^n$ with each element $\Delta_m(i), m = 1,2,.....,n,$ a random number on $[-1,1]$

[Sub step e] Move: Let

$$\theta(i,j+1,k) = \theta(i,j,k) + C(i)\frac{\Delta(i)}{\sqrt{\Delta^T(i)\Delta(i)}}.$$

[Sub step f] Compute $J(i,j+1,k)$.

[Sub step g] Swim: one considers only the i-th bacterium is swimming while the others are not moving then

i) Let $m = 0$ (counter for swim length).

ii) While $m < N_S$ (have not climbed down too long)

- Let $m = m+1$
- If $J(i,j+1,k) < J_{last}$ (if doing better), Let $J_{last} = J(i,j+1,k)$ and let $\theta(i,j+1,k) = \theta(i,j,k) + C(i)\frac{\Delta(i)}{\sqrt{\Delta^T(i)\Delta(i)}}$ and use this $\theta(i,j+1,k)$ to compute the new $J(i,j+1,k)$ as shown in new [sub step f]
- Else, let $m = N_S$. This is the end of the while statement.

[Step 5] Mutation with PSO operator

For i=1, 2,……,S

- Update the $\vec{\theta}_{g\_best}$ and $J_{best}(i,j,k)$
- Update the position and velocity of the d-th coordinate of the i-th bacterium according to the following rule:

$$V_{id}^{new} = \omega V_{id}^{new} + C_1.\varphi_1\left(\theta_{g\_best_d} - \theta_d^{old}(i,j+1,k)\right)$$

$$\theta_d^{new}(i,j+1,k) = \theta_d^{old}(i,j+1,k) + V_{id}^{new}$$

[Step 6] Let $S\_r = S/2$

The S_r bacteria with highest cost function (J) values die and other half bacteria population with the best values split.

[Step 7] If $k < N_{re}$, go to [step 3]. One has not reached the number of specified reproduction steps, so one starts the next generation in the chemotaxis loop.

More details of BF and PSO parameters are presented in Appendix.

5. Results and Simulations

The overall system has been simulated on the digital computer via Simulink tool box in Matlab [60] software package. Fig. 6. shows the variations of objective function with various optimization techniques. The algorithm is run keeping limiting value of cost function at 10^{-6}. It was found that the BSO gives faster convergence than PSO and BF. Moreover, BSO converges at a faster rate (44 generations) compared to that for PSO (68

generations) and BFOA (88 generations). Moreover, computational time (CPU) of both algorithms is compared based on the average CPU time taken to converge the solution. The average CPU for BSO is 43.4 second while it is 68.3 and 79.2 second for PSO and BF respectively.

Table (5), shows the system eigenvalues, and damping ratio of mechanical mode with three different loading conditions. It is clear that the system with BSOSVC has small damping factors (σ=-0.65,-0.69,-1.06) for light, normal, and heavy loading respectively. Moreover, the proposed coordinated controller shifts substantially the electromechanical eigenvalues to the left of the S-plane and the values of the damping factors with the proposed coordinated controller are improved to be (σ=-1.13,-1.17,-1.57) for light, normal, and heavy loading respectively. Also, the damping ratios corresponding to coordinated controller are almost greater than that corresponding to individual ones. Hence compared to the BSOSVC and BSOPSS, the proposed coordinated controller greatly improves the damping characteristics of electromechanical modes. Results of different controllers parameters set values based on the time domain objective function using BF are given in Table (6).

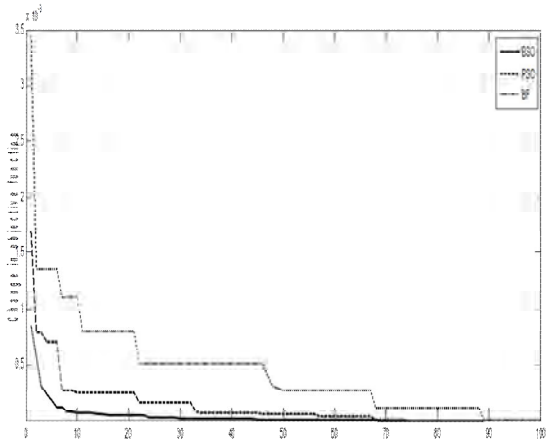

Fig. 6. Change in objective function.

Table (5) Mechanical modes and ζ under different loading conditions and controllers.

	BSOSVC	BSOPSS	Coordinated	Uncoordinated
Light load	-3.1 ± 9.87j, 0.2997 -3.83 ± 7.45j, 0.4572 -0.65 ± 0.79j, 0.6354	-3.76 ± 6.1j, 0.5247 -4.88 ± 6.37j, 0.6081 -0.97 ± 0.67j, 0.8228	-4.74 ± 7.39j, 0.54 -4.98 ± 6.09j, 0.633 -1.13 ± 0.72j, 0.8434	-3.32 ± 9.42j, 0.332 -1.13 ± 6.72j, 0.1658 -0.44 ± 0.75j, 0.50
Norma load	-3.27 ± 11.3j, 0.277 -2.76 ± 9.0j, 0.2932 -0.69 ± 0.78j, 0.6626	-3.95 ± 8.29j, 0.4301 -4.24 ± 6.32j, 0.5571 -0.95 ± 0.74j, 0.7889	-3.98 ± 8.14j, 0.4392 -4.51 ± 6.34j, 0.5797 -1.17 ± 0.63j, 0.8805	-3.01 ± 8.85j, 0.322 -1.21 ± 6.63j, 0.1795 -0.38 ± 0.74j, 0.456
Heavy load	-2.9 ± 11.38j, 0.2461 -1.97 ± 8.78j, 0.2189 -1.06 ± .83j, 0.7873	-3.67 ± 8.42j, 0.398 -3.97 ± 6.55j, 0.5183 -1.08 ± 0.83j, 0.7929	-3.93 ± 8.27j, 0.4292 -4.13 ± 5.9j, 0.5735 -1.57 ± 0.73j, 0.9068	-3.04 ± 8.96j, 0.321 -1.24 ± 6.76j, 0.18 -0.45 ± 0.87j, 0.459

Table (6) Optimal PSSs and SVC parameters.

	Coordinated Design				Uncoordinated Design			
	PSS1	PSS2	PSS3	SVC	PSS1	PSS2	PSS 3	SVC
K	49.51	1.493	1.743	0.915	31.24	8.437	6.38	63.72
T_1	0.465	0.582	0.371	0.371	0.683	0.346	0.25	0.742
T_3	0.268	0.211	0.105	0.288	0.516	0.138	0.33	0.597

A. Response under normal load condition

Figs. 7-8, show the response of $\Delta\omega_{12}$, *and* $\Delta\omega_{13}$ due to severe disturbance is verified by applying a three phase fault of 6 cycle duration at 1.0 second near bus 7. The results of these studies show that the proposed coordinated controller has an excellent capability in damping oscillations and improves the dynamic stability of the power system. Moreover, the settling time of these oscillations is T_s =1.7, 2.0, and 2.2 second for coordinated controller, BSOPSS, and BSOSVC respectively so the designed controller is capable of providing sufficient damping to the system oscillatory modes. Hence, the proposed coordinated controller extends the power system stability limit.

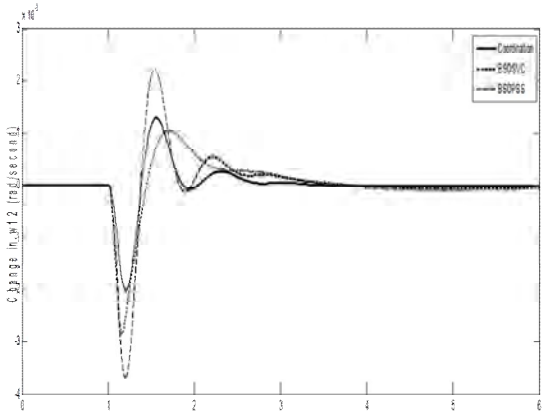

Fig. 7. Change of $\Delta\omega_{12}$ under normal load condition.

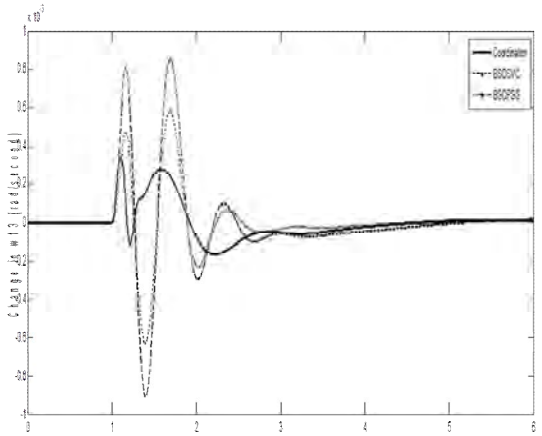

Fig. 8. Change of $\Delta\omega_{13}$ under normal load condition.

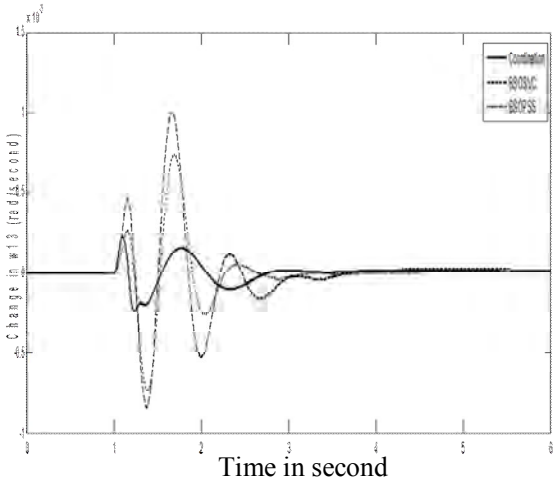

Fig. 10. Change of $\Delta\omega_{13}$ under heavy load condition.

B. Response under heavy load condition

Figs. 9-10, show the system response at heavy loading condition with fixing the controllers parameters. From these Figures, it can be seen that the response with the proposed coordinated controller shows good damping characteristics to low frequency oscillations and the system is more quickly stabilized than BSOPSS and BSOSVC. Moreover, the settling time of these oscillations is T_s=1.7, 2.0, and 2.2 second for coordinated controller, BSOPSS, and BSOSVC respectively. Hence, the simulations results reveal that the simultaneous coordinated designing of the BSOSVC damping controller and the BSOPSS demonstrates its superiority to both the uncoordinated designed controller of the BSOSVC and the BSOPSS. Also, this controller has a simple architecture and the potentiality of implementation in real time environment.

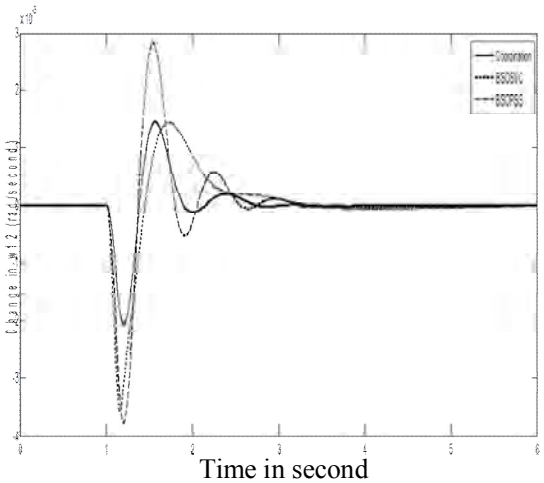

Fig. 9. Change of $\Delta\omega_{12}$ under heavy load condition.

C. Statistical T test

To evaluate the robustness and effectiveness of the proposed coordinated controller, the performance of the system with the proposed coordinated controller is compared to uncoordinated one. A statistical T test is carried out between the coordinated controller and uncoordinated one. The damping ratios of mechanical modes for the coordinated and uncoordinated controller under different loading conditions are selected as input to statistical T test. This test decides that, is there a specific different between two controllers or not?

Let the null hypothesis: $H_0 = \mu_1 - \mu_2 = 0$

Let the alternative hypothesis: $H_1 = \mu_1 - \mu_2 \succ 0$

Where μ_1, μ_2 are the mean values of damping ratios of coordinated and uncoordinated controller respectively. The significance level $\alpha = 0.05$ is established [61-62]. Table (7) shows the output parameters of the statistical T test. The input to the T test is the damping ratios of the mechanical modes for different controllers and operating conditions. The result decides to reject H_0. Also, one can conclude from this test that there is a significant moral difference between the two controllers. Moreover, the response of $\Delta\omega_{12}$ for coordinated and uncoordinated controller is shown in Fig. 11. This Figure indicates the superiority of the proposed coordinated controller in reducing the settling time and damping power system oscillations versus uncoordinated one.

Table (7) Output parameters of statistics T-test.

t-Test: Paired Two Sample for Means	Coordinated	Uncoordinated
Mean	0.647255556	0.324177778
Variance	0.03409811	0.016694377
Observations	9	9
Pearson Correlation	0.646251843	
Hypothesized Mean Difference	0	
df	8	
t Stat	6.861275353	
P(T<=t) one-tail	6.47503E-05	
t Critical one-tail	1.859548033	
P(T<=t) two-tail	0.000129501	
t Critical two-tail	2.306004133	

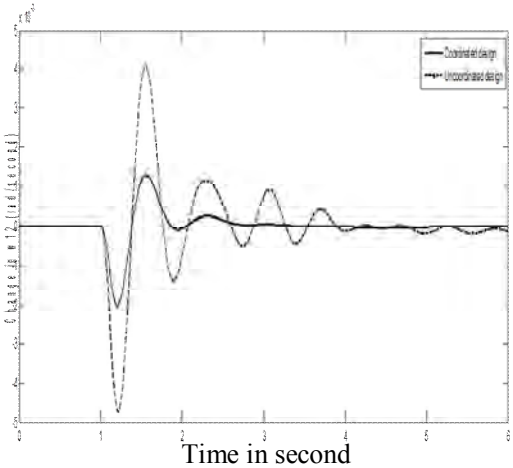

Fig. 11. Comparison between coordinated and uncoordinated design.

6. Conclusions

The statistical assessment of the robust coordinated design of PSSs and SVC damping controller in a multimachine power system is proposed in this paper. The design problem of the proposed controller is formulated as an optimization problem and BSO is employed to search for optimal controller parameters. By minimizing the time domain objective function, in which the deviations in speed are involved; stability performance of the system is improved. Simulations results assure the effectiveness of the proposed coordinated controller in providing good damping characteristic to system oscillations over a wide range of loading conditions and large disturbance. Moreover, it is superior to uncoordinated controller through the statistical assessment.

7. References

[1] P. Kundur, "*Power System Stability and Control*", McGraw-Hill, 1994.

[2] Y. S. Lee, and S. Y. Sun, "*STATCOM Controller Design for Power System Stabilization with Sub-optimal Control and Strip Pole Assignment*", Int. J. of Electrical Power and Energy Systems, Vol. 24, No. 9, November 2002, pp. 771-779.

[3] M. A. Abido, "*Optimal Design of Power System Stabilizers using Particle Swarm Optimization" IEEE Transactions on Energy Conversion*, Vol. 17, No. 3, September 2002, pp. 406-413.

[4] Y.L. Abdel-Magid, and M.A. Abido, "*Coordinated Design of a PSS and a SVC Based Controller to Enhance Power System Stability*", Int. J. of Electrical Power and Energy Systems, Vol. 25, No. 9, November 2003, pp. 695-704.

[5] J. Baskaran, and V. Palanisamy, "*Optimal Location of FACTS Devices in a Power System Solved by a Hybrid Approach*", Int. J. of Nonlinear Analysis, Vol. 65, No. 11, December 2006, pp. 2094-2102.

[6] S. Kodsi, C. Canizares, and M. Kazerani, "*Reactive Current Control Through SVC for Load Power Factor Correction*", Int. J. of Electric Power Systems Research, Vol. 76, No. 9-10, June 2006, pp. 701-708.

[7] S. A. Al-Baiyat, "*Design of a Robust SVC Damping Controller Using Nonlinear* H_∞ *Technique*", The Arabian Journal for Science and Engineering, Vol. 30, No. 1B, April 2005, pp. 65-80.

[8] K. Ellithy, and A. Al-Naamany, "*A Hybrid Neuro-Fuzzy Static Var Compensator Stabilizer for Power System Damping Improvement in the Presence of Load Parameters Uncertainty*", Int. J. of Electric Power Systems Research, Vol. 56, No. 3, December 2000, pp. 211-223.

[9] P. K. Modi , S. P. Singh , and J. D. Sharma, "*Fuzzy Neural Network Based Voltage Stability Evaluation of Power Systems with SVC*", Applied Soft Computing , Vol. 8 , No.1, January 2008, pp. 657-665.

[10] M. H. Haque, "*Best Location of SVC to Improve First Swing Stability of a Power System*", Int. J. of Electric Power System Research, Vol. 77, No. 10, August 2007, pp. 1402-1409.

[11] Y. Chang, and Z. Xu, " *A Novel SVC Supplementary Controller Based on Wide Area Signals*", Int. J. of Electric Power System Research, Vol. 77, No. 12, August 2007, pp. 1569-1574.

[12] S. Panda, N. P. Patidar, and R. Singh, "*Simultaneous Tuning of SVC and Power System Stabilizer Employing Real- Coded Genetic Algorithm*", Int. J. of Electrical and Electronics Engineering, Vol. 4, No. 4, 2009, pp. 240-247.

[13] C. Rakpenthai, S. Premrudeepreechacharn, and S. Uatrongjit, "*Power System with Multi-Type FACTS Devices States Estimation Based on Predictor-Corrector Interior Point Algorithm*", Int. J. of Electrical Power and Energy Systems, Vol. 31, No. 4, May 2009, pp. 160–166.

[14] E. Zhijun, D. Z. Fang, K. W. Chan, and S. Q. Yuan, "*Hybrid Simulation of Power Systems with SVC Dynamic Phasor Model*", Int. J. of Electrical Power and Energy Systems, Vol. 31, No. 5, June 2009, pp. 175–180.

[15] Y. Yuan, G. Li, L. Cheng, Y. Sun, J. Zhang, and P. Wang, "*A Phase Compensator for SVC Supplementary Control to Eliminate Time Delay by Wide Area Signal Input*", Int. J. of Electrical Power and Energy Systems, Vol. 32, No. 3, March 2010, pp. 163-169.

[16] E. S. Ali, "*Static Var Compensator Design for Power System Stabilization Using Bacteria Foraging Optimization Algorithm*", 13th International Middle East Power Systems Conference (MEPCON 2009), Assiut University, Assiut, Egypt, December 20-23, 2009, pp. 578-582.

[17] S. M. Abd-Elazim, and E. S. Ali, "*Bacteria Foraging Optimization Algorithm Based SVC Damping Controller Design for Power System Stability Enhancement*", Int. J. of Electrical Power and Energy Systems, Vol. 43, No. 1, December 2012, pp. 933-940.

[18] X. Y. Bian , C. T. Tse , J. F. Zhang , and K. W. Wang, "*Coordinated Design of Probabilistic PSS and SVC Damping Controllers*", Int. J. of Electrical Power and Energy Systems, Vol. 33, No. 3, March 2011, pp. 445-452.

[19] M. A. Furini, A. L. S. Pereira, and P. B. Araujo, "*Pole Placement by Coordinated Tuning of Power System Stabilizers and FACTS POD Stabilizers*", Int. J. of Electrical Power and Energy Systems, Vol. 33, No. 3, March 2011, pp. 615-622.

[20] S. Panda, "*Multi-objective PID Controller Tuning for a FACTS Based Damping Stabilizer Using Non-dominated Sorting Genetic Algorithm-II*", Int. J. of Electrical Power and Energy Systems, Vol. 33, No. 7, September 2011, pp. 1296-1308.

[21] E. S. Ali, and S. M. Abd-Elazim, "*Coordinated Design of PSSs and TCSC via Bacterial Swarm Optimization Algorithm in a Multimachine Power System*", Int. J. of Electrical Power and Energy Systems, Vol. 36, No. 1, March 2012, pp. 84-92.

[22] A. V. Doroshin, F. Neri, "*Open Research Issues on Nonlinear Dynamics, Dynamical Systems and Processes*", WSEAS Transactions on Systems, 13, 2014, in press.

[23] C. Ciufudean, F. Neri, "*Open Research Issues on Multi-Models for Complex Technological Systems*", WSEAS Transactions on Systems, 13, 2014, in press.

[24] F. Neri, "*Open Research Issues on Computational Techniques for Financial Applications*", WSEAS Transactions on Systems, 13, 2014, in press.

[25] Karthikeyan, P., F. Neri, "*Open Research Issues on Deregulated Electricity Market: Investigation and Solution Methodologies*", WSEAS Transactions on Systems, 13, 2014, in press.

[26] M. Panoiu, F. Neri, "*Open Research Issues on Modeling, Simulation and Optimization in Electrical Systems*", WSEAS Transactions on Systems, 13, 2014, in press.

[27] F. Neri, (2014) "*Open Research Issues on Advanced Control Methods: Theory and Application*", WSEAS Transactions on Systems, 13, in press.

[28] P. Hájek, F. Neri, "*An Introduction to the Special Issue on Computational Techniques for Trading Systems, Time Series Forecasting, Stock Market Modelling, Financial Assets Modelling*", WSEAS Transactions on Business and Economics, Vol. 10, No. 4, 2013, pp. 201-292.

[29] M. Azzouzi, F. Neri, "*An introduction to the special issue on advanced control of energy systems*", WSEAS Transactions on Power Systems, Vol. 8, No. 3, 2013, p. 103.

[30] Z. Bojkovic, F. Neri, (2013) "*An Introduction to the Special Issue on Advances on Interactive Multimedia Systems*", WSEAS Transactions on Systems, Vol. 12, No. 7, pp. 337-338.

[31] L. Pekař, F. Neri, "*An Introduction to the Special Issue on Advanced Control Methods: Theory and Application*", WSEAS Transactions on Systems, Vol. 12, No. 6, 2013, pp. 301-303.

[32] C. Guarnaccia, F. Neri, "*An Introduction to the Special Issue on Recent Methods on Physical Polluting Agents and Environment Modelling and Simulation*", WSEAS Transactions on Systems, Vol. 12, No. 2, 2013, pp. 53-54.

[33] F. Neri, "*An Introduction to The Special Issue on Computational Techniques for Trading*

Systems, Time Series Forecasting, Stock Market Modelling, and Financial Assets Modelling", WSEAS Transactions on Systems, Vol. 11, No. 12, 2012, pp. 659-660.

[34] M. Muntean, F. Neri, "*Foreword to the Special Issue on Collaborative Systems*", WSEAS Transactions on Systems, Vol. 11, No. 11, 2012, p. 6.

[35] L. Pekař, F. Neri, "*An Introduction to the Special Issue on Time Delay Systems: Modelling, Identification, Stability, Control and Applications*", WSEAS Transactions on Systems, Vol. 11, No. 10, 2012, pp. 539-540.

[36] C. Volos, F. Neri, "*An Introduction to the Special Issue: Recent Advances in Defence Systems: Applications, Methodology, Technology*", WSEAS Transactions on Systems, Vol. 11, No. 9, 2012, pp. 477-478.

[37] J. Kennedy and R. Eberhart, "*Particle Swarm Optimization*", Proceedings of IEEE International Conference on Neural Networks, 1995, pp. 1942-1948.

[38] D. P. Rini, S. M. Shamsuddin, and S. S. Yuhaniz, "*Particle Swarm Optimization: Technique, System and Challenges*", Int. J. of Computer Applications, Vol. 14, No. 1, January 2011, pp. 19-27.

[39] V. Selvi and R. Umarani, "*Comparative Analysis of Ant Colony and Particle Swarm Optimization Techniques*", Int. J. of Computer Applications, Vol. 5, No. 4, August 2010, pp. 1-6.

[40] A. S. Oshaba, and E. S. Ali, "*Speed Control of Induction Motor Fed from Wind Turbine via Particle Swarm Optimization Based PI Controller*", Research Journal of Applied Sciences, Engineering and Technology, Vol. 5, No. 18, May 2013, pp. 4594-4606.

[41] A. S. Oshaba, and E. S. Ali, "*Swarming Speed Control for DC Permanent Magnet Motor Drive via Pulse Width Modulation Technique and DC/DC Converter*", Research Journal of Applied Sciences, Engineering and Technology, Vol. 5, No. 18, May 2013, pp. 4576-4583.

[42] K. M. Passino, "*Biomimicry of Bacterial Foraging for Distributed Optimization and Control*", IEEE. Control System Magazine, Vol. 22, No. 3, June 2002, pp. 52-67.

[43] S. Mishra, "*A Hybrid Least Square Fuzzy Bacteria Foraging Strategy for Harmonic Estimation*", IEEE Trans. Evolutionary Computer, Vol. 9, No.1, February 2005, pp. 61-73.

[44] D. B. Fogel, "*Evolutionary Computation towards a New Philosophy of Machine Intelligence*", IEEE, New York, 1995.

[45] E. S. Ali and S. M. Abd-Elazim, "*Bacteria Foraging Optimization Algorithm Based Load Frequency Controller for Interconnected Power System*", Int. J. of Electrical Power and Energy Systems, Vol. 33, No. 3, March 2011, pp. 633-638.

[46] E. S. Ali, and S. M. Abd-Elazim, "*TCSC Damping Controller Design Based on Bacteria Foraging Optimization Algorithm for a Multimachine Power System*", Int. J. of Electrical Power and Energy Systems, Vol. 37, No. 1, May 2012, pp. 23-30.

[47] E. S. Ali, and S. M. Abd-Elazim, "*Power System Stability Enhancement via Bacteria Foraging Optimization Algorithm*", Int. Arabian Journal for Science and Engineering, Vol. 38, No. 3, March 2013, pp. 599-611.

[48] S. M. Abd-Elazim, and E. S. Ali, "*Optimal Power System Stabilizers Design for Multimachine Power System Using Hybrid BFOA-PSO Approach*", Int. J. of WSEAS Transactions on Power Systems, Vol. 8, No. 2, April 2013, pp. 85-94.

[49] S. M. Abd-Elazim, and E. S. Ali, "*Synergy of Particle Swarm Optimization and Bacterial Foraging for TCSC Damping Controller Design*", Int. J. of WSEAS Transactions on Power Systems, Vol. 8, No. 2, April 2013, pp. 74-84.

[50] E. S. Ali, S. M. Abd-Elazim, "*BFOA based Design of PID Controller for Two Area Load Frequency Control with Nonlinearities*", Int. J. of Electrical Power and Energy Systems, Vol. 51, 2013, pp. 224-231.

[51] E. S. Ali, S. M. Abd-Elazim, "*Optimal PSS Design in a Multimachine Power System via Bacteria Foraging Optimization Algorithm*", Int. J. of WSEAS Transactions on Power Systems, Vol. 8, No. 4, October 2013, pp. 186-196.

[52] E. S. Ali, S. M. Abd-Elazim, "*Hybrid BFOA-PSO Approach for Optimal Design of SSSC Based Controller*", Int. J. of WSEAS Transactions on Power Systems, Vol. 9, No. 1, January 2014, pp. 54-66.

[53] A. Biswas, S. Dasgupta, S. Das, and A. Abraham, "*Synergy of PSO and Bacterial Foraging Optimization: A Comparative Study on Numerical Benchmarks*", Innovations in Hybrid Intelligent Systems, ASC 44, 2007, pp. 255-263.

[54] W. Korani, "*Bacterial Foraging Oriented by Particle Swarm Optimization Strategy for PID Tuning*", GECCO'08, July 12-16, 2008, Atlanta, Georgia, USA, pp. 1823-1826.

[55] P. Kundur, M. Klein, G. J. Rogers, and M. S. Zywno, "*Application of Power System Stabilizers for Enhancement of Overall System Stability*", IEEE Trans. Power System, Vol. 4, No. 2, 1989, pp. 614-626.

[56] E. S. Ali, "*Optimization of Power System Stabilizers Using BAT Search Algorithm*", Int. J. of Electrical Power and Energy Systems, Vol. 61, No. C, October 2014, pp. 683-690.

[57] P. M. Anderson and A. A. Fouad, "*Power System Control and Stability*", Iowa State University Press, Iowa, 1977.

[58] S. M. Abd- Elazim, "*Comparison between SVC and TCSC Compensators on Power System Performance*", Master thesis, 2006, Zagazig University, Egypt.

[59] S. M. Abd-Elazim, and E. S. Ali, "*A Hybrid Particle Swarm Optimization and Bacterial Foraging for Power System Stability Enhancement*", IEEE, 15th International Middle East Power Systems Conference "MEPCON'12", Alexandria University, Egypt, December 23-25, 2012.

[60] The MathWorks, Inc. ,"*MATLAB Simulink Toolbox*", Version 7.10 (R2010a), MATLAB Software.

[61] S. M. Ross, "*Introduction to Probability and statistics for Engineers and Scientists*", 3rd edition, Elsevier Academic Press, 2004.

[62] W. L. Martinez, and A. R. Martinez, "*Computational Statistics Handbook with MATLAB*", Chapman & Hall/CRC, 2002.

Appendix

The system data are as shown below:

The system data	
Excitation system	$K_A = 400$; $T_A = 0.05$ second; $K_f = 0.025$; $T_f = 1$ second.
SVC Controller	$T_r = 15$ msecod ; K_r =50; $\alpha 0$ =140.
Bacteria parameters	Number of bacteria =10; number of chemotatic steps =10; number of elimination and dispersal events = 2; number of reproduction steps = 4; probability of elimination and dispersal = 0.25; the values of $d_{attract}$ =0.01; the values of $\omega_{attract}$ =0.04; the values of $h_{repelent}$ =0.01; the values of $\omega_{repelent}$ =10.
PSO parameters	$C_1 = C_2$ =2.0, ω =0.9.

The influence of home nonlinear electric equipment operating modes on power quality

ANGELA IAGAR GABRIEL NICOLAE POPA CORINA MARIA DINIS
Department of Electrotechnical Engineering and Industrial Informatics
Politehnica University Timisoara
Revolutiei str., no.5, 331128, Hunedoara
ROMANIA
angela.iagar@fih.upt.ro http://www.fih.upt.ro/v3/

Abstract: - The proliferation of nonlinear electronic loads is increasing day by day, and it can anticipate an influx of newer technologies in this domain in the future. This article focuses on the impacts of various home nonlinear electric equipment on the power quality of electrical distribution system. It was studied the influence of operating mode on the harmonic pollution generated by nonlinear home appliances operating in an isolated mode, using the *CA 8334B* three-phase power quality analyzer. Although home electric appliances are low power receivers, the cumulative effect produced by a large number of small harmonic sources can be substantial.

Key-Words: -disturbances, harmonics, nonlinear equipment, operating mode, power quality

1 Introduction

Harmonic distortions are the major cause for power quality problems [1, 2].

In recent years many studies have as subject the power quality problems caused by nonlinear loads on the electric power grid. When fed directly from the utility power system, nonlinear loads generally have non-sinusoidal harmonic currents [2].

Power electronics equipment, such as adjustable speed drives, controlled rectifiers, cyclo-converters, arc furnaces, induction heating equipment,electronically ballasted lampsand clusters of personal computers, represent major nonlinear and parametric loads proliferating among industrial and commercial customers [3-16]. In addition, the proliferation of nonlinear home electric appliances is increasing day by day.

Nonlinear loads have the potential to create disturbances for the utility and the end-user's equipment. Non-sinusoidal harmonic currents can lead to significant line voltage distortion [17-21]. Also, harmonics can interfere with control, communication or protection equipment, causing energy meter inaccuracy, additional losses and decreasing the equipment lifetime. Harmonic distortion degrades the power factor. The flow of non-active energy caused by harmonic currents and voltages became a great problem today [1, 2,17].

Home electric appliances, although they are relatively low-power receivers, summed can represent an important source of harmonic distortion, because it can be used at the same time a large number of receivers over long periods of time.

For example, measurements carried out on a sample of 50 power substations in France during one day, show that the highest rate of 5^{th} voltage harmonic order is, in general, between 12-14 hours and 20-22 hours, due to home nonlinear electric equipment [22].

During the last years large numbers of compact fluorescent lamps (*CFLs*) penetrate the market place. *CFL*s provide significant energy saving comparable with incandescent lamps. But, *CFL*s create harmonics on the supply system because of the control systems limiting the plasma current, which produces light [17, 23]. Electronic ballast has a switched mode power supply (*SMPS*) to convert the fundamental frequency to a higher frequency, usually around 25-40 *kHz* [24]. A small inductor is also used in the electronic type to limit the current.

Several studies reveal that the distortion level depends on the type of *CFL* used and the distribution parameter. The currents distortion for the *CFL* may be very high, even when *CFL* is 10% of the total load, can result an unacceptable voltage distortion at the point of common coupling (*PCC*) [23, 24].

Within the next 10 years the displacement of *CFL*s by solid state lamps (*SSL*s) is most likely. Also, electric vehicles are expected to be part of distribution systems at a massive scale. Therefore, the study of harmonic pollution must predict the

impact of new power electronic equipment in the electric power grid, because the harmonic distortion may become critical.

When several identical loads share the same source impedance may appear the effect of attenuation, consisting of reduction in harmonic magnitude, and change in phase angle. The effect of diversity describes a reduction, or even cancellation of harmonics due to loads of different levels, or connected through different impedances, presenting differing phase angles to the supply [25, 26].

This article presents the influence of operating mode on the power quality disturbances of home nonlinear equipment, especially harmonic pollution. It was studied the impacts of various home nonlinear electric equipment operating in an isolated mode. Further study is required to establish the impacts of these loads operating together.

2 Laboratory measurements

In order to comply with *EMC* standards the end-users have to guarantee current absorptions with adequate power factor (*PF*) and reduced harmonic current [1, 2]. An inadequate *PF* (lower than neutral value) increase very much the power losses in the distribution grid, the voltage drop and the voltage distortion [2].

Typical nonlinear home appliances contain electromagnetic devices, such as motors and transformers (e.g. refrigerators and air-conditioning devices). The current distortion depends on the motor's design and varies with the voltage level. These nonlinear loads should be modeled by harmonic current sources [18, 19].

Other nonlinear loads should be modeled by harmonic voltage sources. Among such loads are diode rectifiers with capacitive output (*DC*) filters, which are the usual interface between electronic loads and the *AC* feeder. This kind of circuit (*SMPS*) is present in almost all residential and commercial nonlinear loads, such as computers, monitors, TV sets, electronic ballasts for fluorescent lamps, battery chargers, etc. [19].

The laboratory measurements were made using a power quality analyzer *CA 8334B*. To measure the current was used current probes *MN 93A* (5 *A* and 200 *A*) [27].

The main parameters measured by *CA 8334B* analyzer were: *True RMSAC* phase voltages and *True RMSAC* line currents; peak voltage and current; active, reactive and apparent power per phase; power factor, displacement power factor; harmonics for voltages and currents up to the 50th order; Fresnel diagrams.

Below are presented the results of measurements for the following home nonlinear equipment: refrigerator, microwave oven, induction heat plate, personal computer, laptop, laser printer,air-condition device, compact fluorescent lamps, operating in an isolated mode.

2.1 Refrigerator

In the laboratory measurements was used a low-power refrigerator.

Fig.1 shows the supply voltage and current from a refrigerator. Voltage waveform is very close to the sinusoidal; this is confirmed by harmonic spectrum from Fig.2, total harmonic distortion (THD_U) of supply voltage being 4.9%, according to *EMC* standards [28, 29].

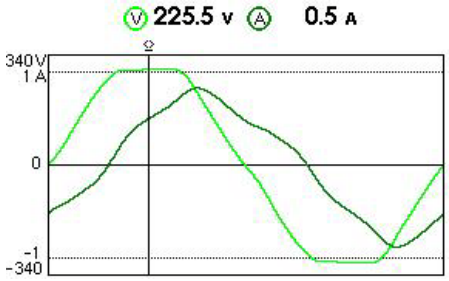

Fig.1 Refrigerator's voltage and current.

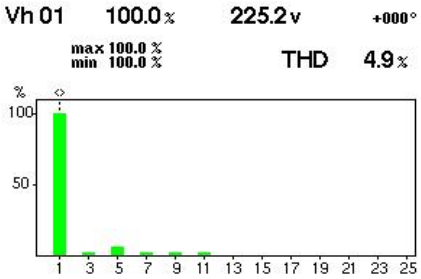

Fig.2 Harmonic spectrum of supply voltage.

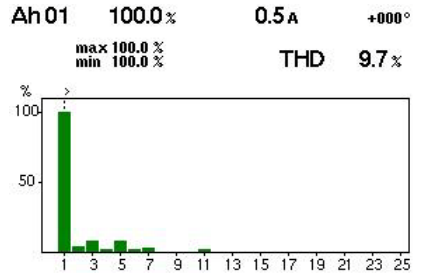

Fig.3 Harmonic spectrum of refrigerator's current.

THD of the refrigerator current is 9.7% (Fig.3), and exceed the compatibility limits. Also, the 3rd and 5th harmonics exceed the compatibility limits.

In the case of refrigerator, the average value of power factor*PF*(defined as ratio of the active power to the apparent power) is very poor (PF_{avg}=0.57, maximum value being PF_{max} =0.679).

Also, displacement power factor *DPF* (defined as the cosine of the angle between the fundamental components of the voltage and the current) is very small and approximately equal to *PF* ($DPF_{avg}=0.573$ and $DPF_{max}=0.685$). This indicates a very high reactive power consumption and relatively low harmonic current distortion.

2.2 Microwave oven

2.2.1 No-load operation

When microwave oven operating without load, the supply voltage is very close to sine wave; THD_Udoes not exceed the compatibility limits (Figs.4, 5). Operation time was 30 *s*.

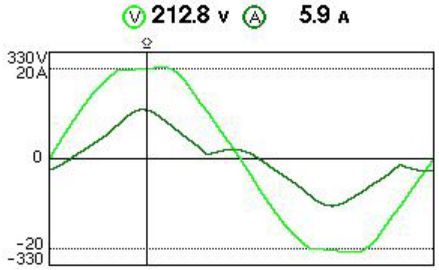

Fig.4 Microwave oven's voltage and current (no-load operation).

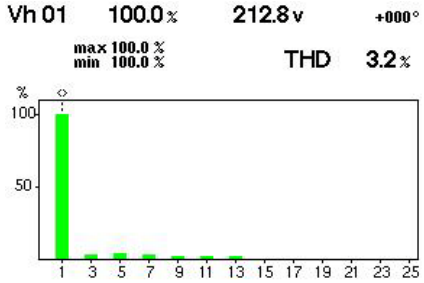

Fig.5 Harmonic spectrum of supply voltage.

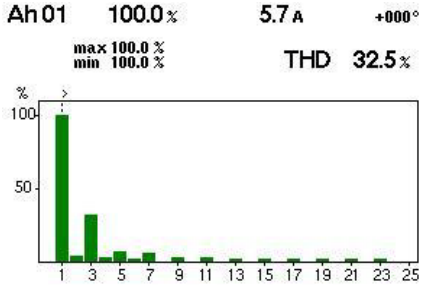

Fig.6 Harmonic spectrum of microwave oven's current (no-load operation).

The current waveform from microwave oven in no-load operation is highly distorted as compared to ideal sine wave and has a THD_Ivalue of 32.5 %. The 3rd, 5th, 7th harmonics have values higher than the maximum standard values.

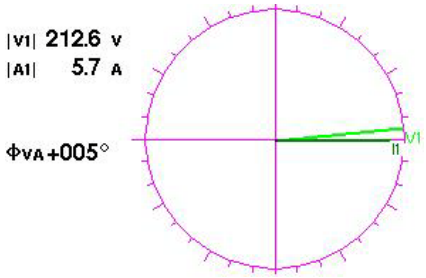

Fig.7 Fresnel diagram for voltage and current (microwave ovenno-load operation).

Fresnel diagram (Fig.7) indicates the inductive nature of microwave oven and a very small phase angle deviation (5°) between voltage and current is present. Therefore power factors are very good and exceed the neutral value (*PF=0.951* and *DPF=0.999*). The difference between *PF* and *DPF* indicates a large deviation from sinusoidal waveform of current.

2.2.2 Load operation

Measurement results when microwave oven was in load operation are presented in Figs.8, 9 and Table 1. Operation time was 30 *s*.

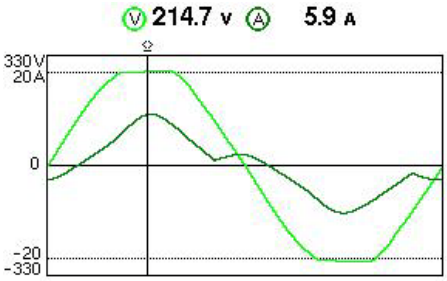

Fig.8 Microwave oven's voltage and current (load operation, 4 pancakes).

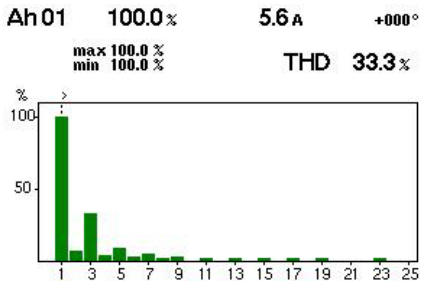

Fig.9 Harmonic spectrum of microwave oven's current (load operation, 4 pancakes).

It is found that microwave load influence very little its operation (Table 1). When the oven load increases, the current and voltage harmonic distortions slightly increase, and power factors slightly decrease.

In all situations $THD_I$and 3rd, 5th, 7th harmonics levels exceed the compatibility limits, but THD_U is small; powers factor exceed the neutral value.

Table 1 - Load operation of microwave oven

Load	THD_U [%]	THD_I [%]	PF [-]	DPF [-]
1 pancake	2.9	30.8	0.95	0.999
2 pancakes	2.9	31	0.948	0.997
4 pancakes	3.2	33.3	0.928	0.985
mashed potatoes	3.3	33.2	0.932	0.987
empty vessel	3.2	30.4	0.952	0.997

2.3 Induction heat plate

The loads of induction heat plate were two steel kettles with different amounts of water. The first kettle had a base diameter of 8 cm; the second kettle (stainless steel) had a diameter of 12 cm.

2.3.1 Load operation

Figs. 10-17 and Table 2 present the results of measurements for an induction heat plate at various loads. Active power was set at 1600 *W*.

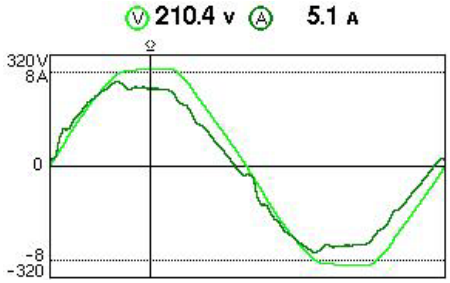

Fig.10 Induction heat plate's voltage and current(load operation,first kettle, 470 *ml* water).

Supply voltage and current are very close to sine wave when induction heat plate has the first steel kettle with 470 *ml* water as load. Total harmonic distortions are very small (THD_U=2.6 *%*,THD_I=6.2 *%*); all harmonics have values smaller than the maximum standard values.

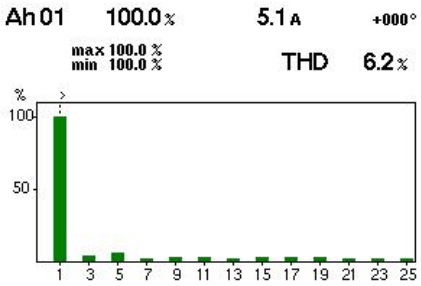

Fig.11 Harmonic spectrum of induction heat plate's current (load operation, firstkettle, 470 *ml* water).

Fresnel diagram (Fig.12) shows the capacitive nature of induction heat plate and a small phase angle deviation (10°) between voltage and current is present. Power factors exceed the neutral value (PF=0.985, DPF=0.986), and are approximately equal (due to low harmonic distortion of current and voltage).

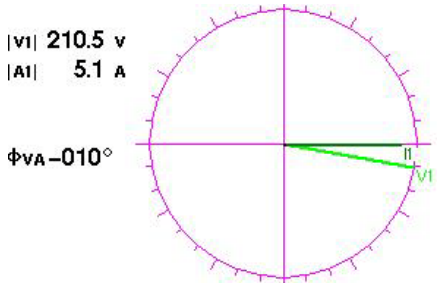

Fig.12 Fresnel diagram for induction heat plate's voltage and current (load operation, first kettle, 470 *ml* water).

Fig.13Induction heat plate's voltage and current (load operation, secondkettle, 470 *ml* water).

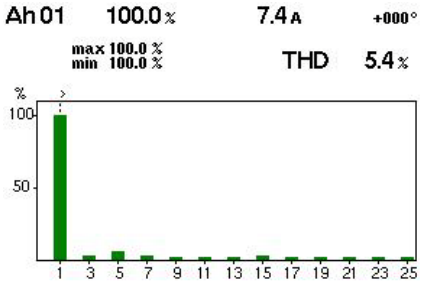

Fig.14 Harmonic spectrum of induction heat plate's current (load operation, second kettle, 470 *ml* water).

Figs. 13, 14 show that although stainless steel kettle (12 *cm*) had the same amount of water as that of steel (8 *cm*), the current (*RMS* value) from induction heat plate is much higher than in the previous case (7.4 *A*). Total harmonic distortion of the voltage increases slightly, but in the case of current decreases (THD_U=2.8 *%*,THD_I=5.4 *%*). It also decreases the phase difference between voltage and current (6°), and power factors are higher than in the previous case (PF = 0.993, DPF = 0.994).

In conclusion, the load of the induction heat plate depends on cooking vessel and does not depends on vessel's contents, which is evident by Table 2.

In Table 2 the load was stainless steel kettle (12 *cm*) with various amounts of water. Content of the kettle influence insignificant the induction heat

plate's current, active, reactive and apparent powers (*P*, *Q*, *S*), THD_U, THD_I, *PF* and *DPF*.

Table 2 - Load operation of induction heat plate

Stainless steel kettle	940*ml* water	705 *ml* water	470*ml* water	235*ml* water
P [*W*]	1550	1553	1549	1547
Q [*VAR*]	179	179	179	179
S [*VA*]	1564	1556	1559	1558
PF [-]	0.993	0.993	0.993	0.993
DPF [-]	0.994	0.994	0.994	0.994
THD_U [%]	2.8	2.8	2.8	2.6
THD_I [%]	5.4	5.4	5.4	5.3
t [*s*]	150	110	70	42

Table 2 shows the great efficient of induction heat plate, time required for boiling water (*t*) in each case being very small.

2.3.2 Stand-by operation

Although the induction heat plate at load operation is compatible electromagnetic, after pressing stop switch (stand-by operation) it was find a pronounced distortion of the current (Figs.15, 16).

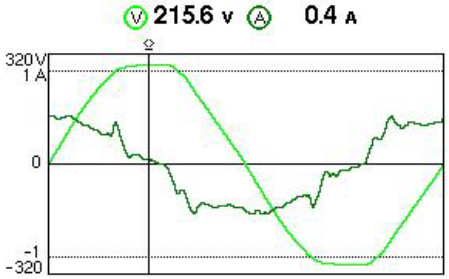

Fig.15 Induction heat plate's voltage and current (stand-by operation).

In stand-by, the harmonic distortion of supply voltage remains very low (THD_U=2.6 %), but THD_Ihas a high value, equal to 17.7%; 3rd, 5th, 7th, 9th, 13th, 15th, 17th, 19th, 21st, 23rd, 25th current harmonics breaching the standard limits. Active, reactive, apparent powers and power factors in stand-by operation were: *P*=6.4 *W*, *Q*=82.2 *VAR*, *S*=22.5 *VA*,
PF=0.078, *DPF*=0.078.

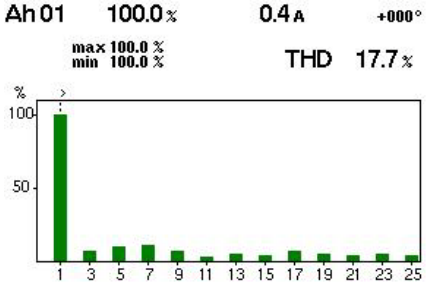

Fig.16 Harmonic spectrum of induction heat plate's current (stand-by operation).

2.4 Personal computer

Personal computers (*PC*s) impacts on power quality due to the using of *SMPS* for converting single phase *AC* into low voltage *DC* for supplying electronics devices [30].

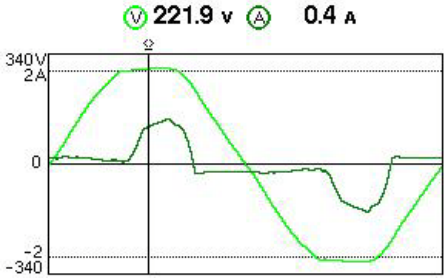

Fig.17 PC and monitor's voltage and current (idle mode).

Because the capacitor of *SMPS* is charged only during the peak of the voltage waveform, large current pulse appears in the current from *PC* at the peak of the voltage waveform [23].

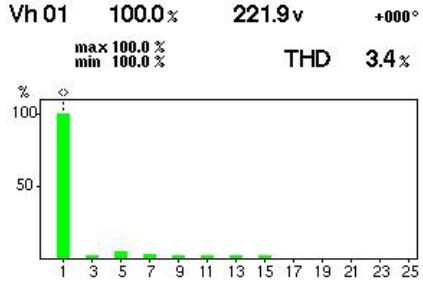

Fig.18 Harmonic spectrum of voltage supply (idle mode).

The current from *PC* (*Dell*) and *LCD* monitor is highly distorted (THD_I=91.5 %); 3rd, 5th, 7th, 9th, 11th, 13th, 15th, 17th, 19th, 21st, 23rd, 25th current harmonics exceed the standard limits (3rd harmonic level exceeds 80%). $THD_U$is in the acceptable standard limit, being equal to 3.4%.

Average values of active, reactive, apparent powers and power factors in idle mode of *PC* were: *P*=72.3 *W*, *Q*=66.2 *VAR*, *S*=98 *VA*, *PF*=0.738, *DPF*=0.993.

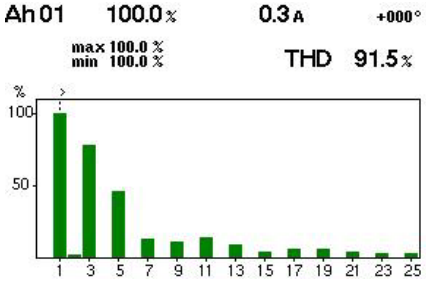

Fig.19 Harmonic spectrum of *PC* and monitor's current (idle mode).

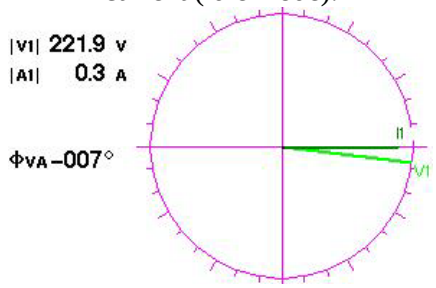

Fig.20 Fresnel diagram for *PC* and monitor's voltage and current (idle mode).

Fresnel diagram (Fig.20) indicates the capacitive nature of *PC* and monitor in idle mode operation.

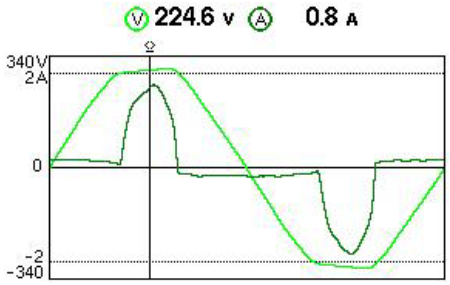

Fig.21*PC* and monitor's voltage and current (hard disk drive access).

Fig.21 shows the waveforms of *PC* and monitor's voltage and current when a small file is reading on local hard disk (*HD*). In this operational mode (*HD* drive access) the *RMS* value of current drawn by *PC* and monitor increases compared to idle mode operation.

Large concentrations of *PC*s are increasingly found in high density residential areas, offices, classrooms, etc. Several studies have shown that the current harmonics from a single *PC* differed considerably to the harmonics generated collectively by several *PC*s of the same type [31-33]. For example, when many *PC*s are operating in parallel from the same bus a significant reduction in line current harmonics may occurs (diversity effect).

2.5 Laptop

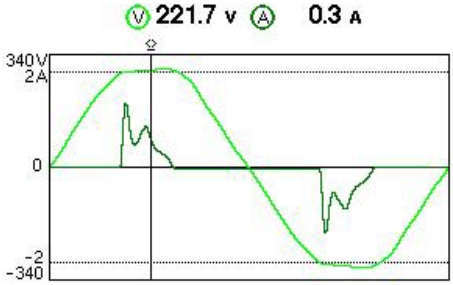

Fig.22 Laptop's voltage and current (charging mode).

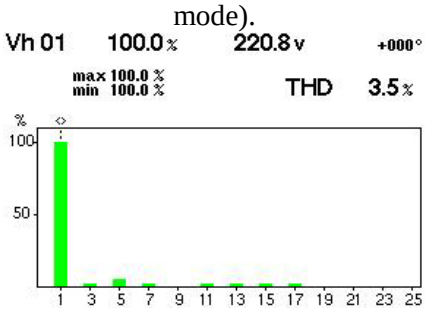

Fig.23 Harmonic spectrum of voltage supply (charging mode of laptop).

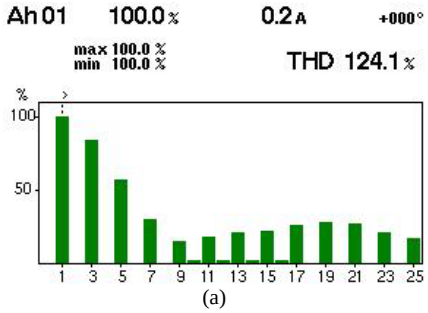

(a)

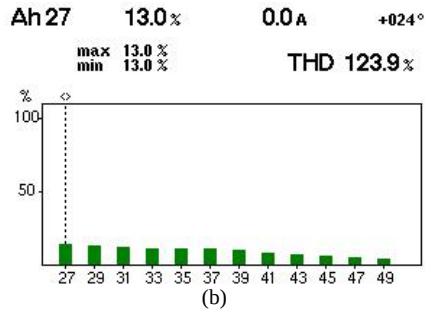

(b)

Fig.24 Harmonic spectrum of laptop's current (charging mode).

In the charging mode of laptop (*Lenovo*) THD_U is less the acceptable standard limit (THD_U=3.5%).THD_I has an alarmingly high value, equal to 124%.

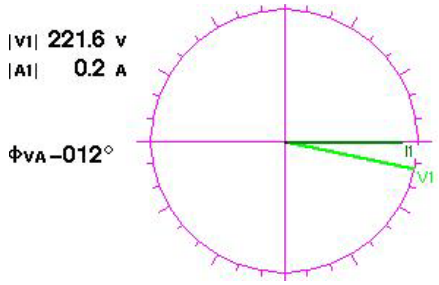

Fig.25 Fresnel diagram for laptop's voltage and current (charging mode).

In charging mode of laptop all odd harmonics of the current exceed the standard limits (3rd and 5th harmonic levels exceed 80%, respectively 60%).

Fresnel diagram (Fig.25) indicates the capacitive nature of laptop in charging mode. Average values of active, reactive, apparent powers and power factors in charging mode of laptop were: *P*=44.2 *W*, *Q*=59.1 *VAR*, *S*=73.8 *VA*, *PF*=0.598, *DPF*=0.976. Power factor is very small, less than neutral value.

In operating mode of laptop the *RMS* value of current increases compared to charge mode (Fig.26).

Fig.26 Laptop's voltage and current (operating mode).

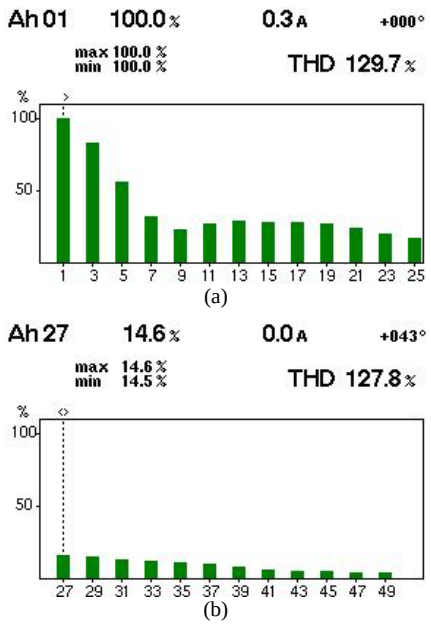

Fig.27 Harmonic spectrum of laptop's current (operating mode).

Voltage waveform remains very close to the sinusoidal (THD_U=3.5%); THD_Iincreases even more compared to charging mode, being equal to 129.7%; all odd harmonics of the current exceed very much the standard limits in this case (Fig.27).

Average values of active, reactive, apparent powers and power factors in operating mode of laptop were: *P*=61.2 *W*, *Q*=89.9 *VAR*, *S*=108.9 *VA*, *PF*=0.563(capacitive), *DPF*=0.973. Power factors slightly decrease compared to charging mode. *PF* has an inadequate value. The large differencebetween *PF* and *DPF* indicates the highly distorted current drawn by laptop.

2.6 Laser printer

Figs.28-30 show that voltage supply does not exceed the compatibility limits in the idle mode of laser printer (THD_U=4.8%),but current waveform is highly distorted (THD_I=89.8%); all odd harmonics exceed very much the standard limits.

Fig.28 Laser printer's voltage and current (idle mode).

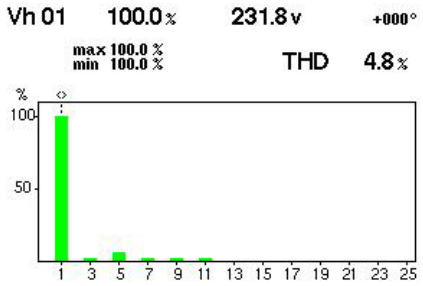

Fig.29 Harmonic spectrum of voltage supply (laser printer in idle mode).

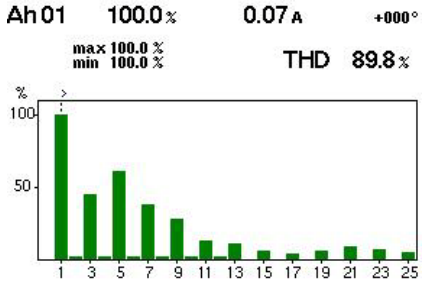

Fig.30 Harmonic spectrum of laser printer's current (idle mode).

3rd, 5th, 7th, 9th, 11th, 13th harmonics have very large levels: 45%, 60%, 37%, 29%, 14%, 12%.Average values of active, reactive and apparent powers in idle mode of laser printer were: *P*=73.4 *W*, *Q*=210.2 *VAR*, *S*=222.7 *VA*. Power factors are very small, less than neutral value(*PF*=0.329, *DPF*=0.441).

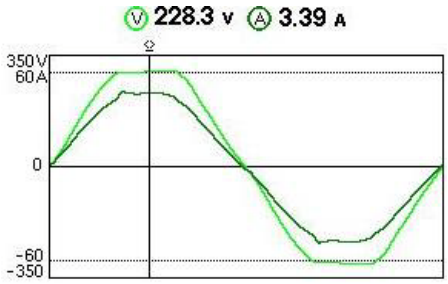

Fig.31 Laser printer's voltage and current (printing mode).

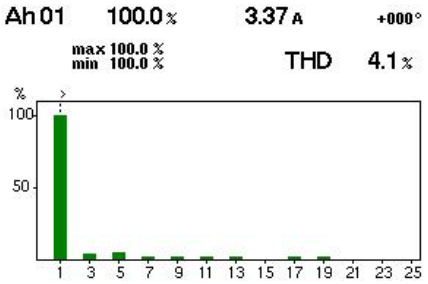

Fig.32 Harmonic spectrum of laser printer's current (printing mode).

Supply voltage and current are very close to sine wave in the printing mode. In this mode the printer works as a resistive load. Voltage and current distortions are within the acceptable standard limits in this case (THD_U=4.8%, THD_I=4.1%).

2.7 Air-condition device

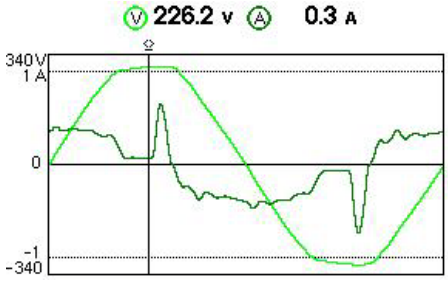

Fig.33 Air-condition device's voltage and current (stand-by mode).

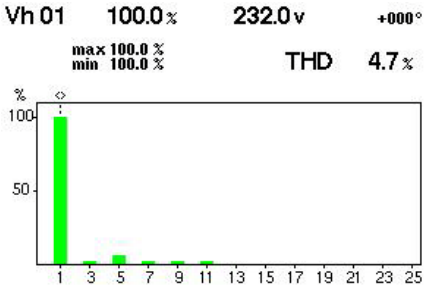

Fig.34 Harmonic spectrum of voltage supply (air-condition device in stand-by).

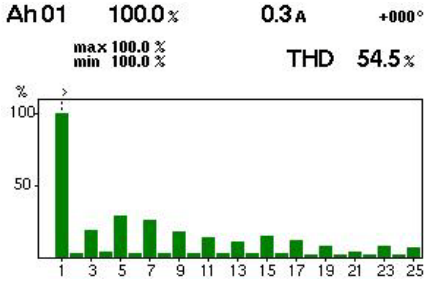

Fig.35 Harmonic spectrum of air-condition device's current (stand-by mode).

In stand-by mode of air-condition device waveform of voltage supply is very little distorted (THD_I=4.7%), but current waveform is very high distorted (THD_I=54.5%). All odd current harmonics exceed the compatibility limits.

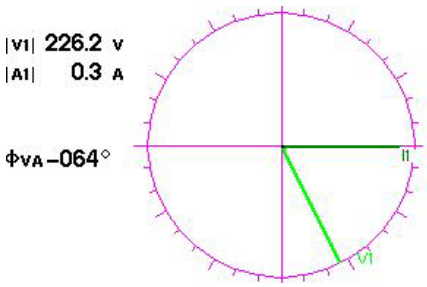

Fig.36 Fresnel diagram for voltage and current (air-condition device in stand-by).

Average values of active, reactive and apparent powers in stand-by mode of air-condition device were: *P*=121.4 *W*, *Q*=210.6 *VAR*, *S*=235.3 *VA*. Fresnel diagram (Fig.36) indicates the capacitive nature of air-condition device in stand-by mode. Power factor are very poor and less than neutral value(*PF*=0.516). The large difference between *PF* and *DPF* indicates the highly distorted current drawn by air-condition device in this case (*DPF*=0.941).

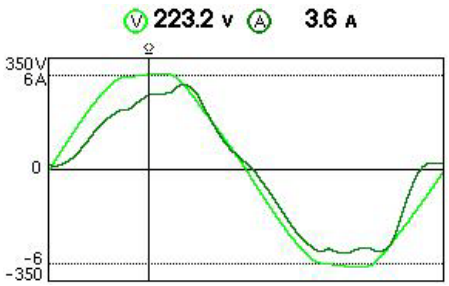

Fig.37 Air-condition device's voltage and current (heating mode).

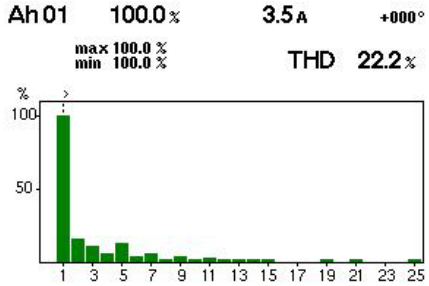

Fig.38 Harmonic spectrum of air-condition device's current (heating mode).

In heating mode of air-condition device waveform of voltage supply remain approximately sinusoidal (Fig.37); current distortion is significantly reduced in this mode of operation (Fig.38, THD_I=22.2%). Fresnel diagram (Fig.39) shows the inductive nature of air-condition device in heating mode, and a small phase angle deviation (4°) between voltage and current.

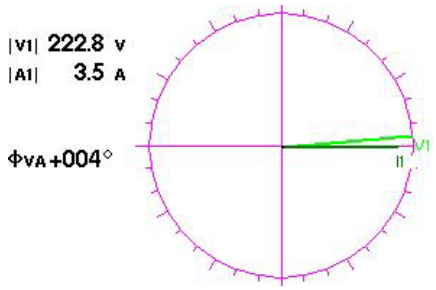

Fig.39 Fresnel diagram for air-condition device's voltage and current (heating mode).

2.8 Compact fluorescent lamps (CFLs)

Were analysed three CFLs with rated power of 15W (two CFLs) and 20W connected in parallel.

Fig.40 CFLs supply voltage and current.

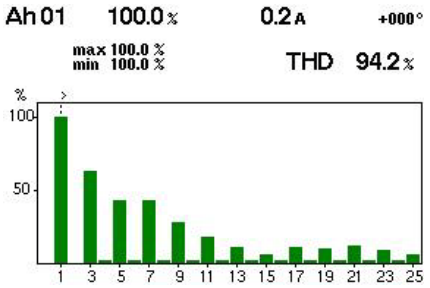

Fig.41 Harmonic spectrum of CFLs current.

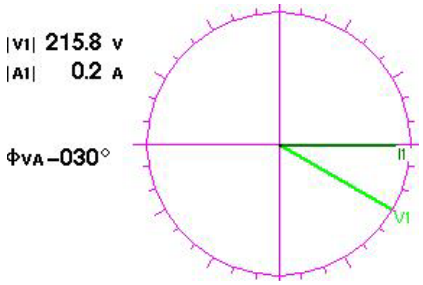

Fig.42 Fresnel diagram for voltage and current of CFLs.

Total current absorbed by CFLs is highly distorted (THD_I=94.2%); all odd harmonics of the current exceed the standard limits (3rd, 5th, 7th, 9th harmonic levels exceed 60%, 40% and 25%).

Fresnel diagram (Fig.42) indicates the capacitive nature of CFLs. Average values of active, reactive and apparent powers were: P=48.2W, Q=55.5VAR, S=73.5VA. Power factors are very small(PF=0.656, DPF=0.894), less than neutral value.

3 Conclusion

Most of the nonlinear electric equipment highly distorted current waveforms which produces high levels of harmonic distortions when connected to a distribution system.

*SMPS*is present in almost all home and commercial nonlinear loads, such as computers, monitors, laptops, electronic ballasts for fluorescent lamps, etc. From all house nonlinear electric equipment, these type of loads show the most current harmonic distortion.

SMPS's current has a significant amount of multiply 3rd harmonics order (3rd, 9th, 15th, etc.). Multiply 3rd order harmonics are zero sequence. These harmonics add algebraically through neutral conductor.

So, in three-phase power systems that have a neutral conductor and a large number of single-phase *SMPS* loads, even if the loads are balanced (on the three phases), will circulate an important neutral current, that can not be eliminated or reduced.

Current harmonic distortion is influenced by operation mode for almost analysed nonlinear loads, with the exception of the microwave oven.

Induction heat plate generates harmonics only in stand-by mode, the laser printer only in idle mode and the air condition devices, especially in stand-by mode. Due to the nonlinear electronics equipment show that harmonic voltage distortion is up 4.9 %.

In these conditions the following adverse effects may occur:

-losses in power transformer from power station may increase at 25%;

-available power of power station may be reduced by approximately 10-15%.

The cumulative effect produced by a large number of small nonlinear electric equipment (harmonic sources) can be substantial, because the total harmonic distortion current (THD_I) can reach up to 130% at the terminals of these electric loads, generating additional power and energy losses in electric networks.

References:

[1] J. Arrillaga and N. R. Watson, *Power System Harmonics*, John Wiley&Sons, Ltd., West Sussex, England, 2003.

[2] ***, *Power Quality Application Guide*, Copper Development Association, U.K., 2001.

[3] M. Panoiu, C. Panoiu, M. Osaci, I. Muscalagiu, Simulation Result about Harmonics Filtering using Measurement of Some Electrical Items in Electrical Installation on UHP EAF, *WSEAS Transactions on Circuits and Systems*, Vol. 7, No.1, January 2008, pp. 22-31.

[4] R. Rob, I. Sora, C. Panoiu, M. Panoiu, Harmonic filters influences regarding the power quality on high frequency electrothermal installation with electromagnetic induction, *WSEAS Transactions on Systems*, Vol. 9, No.1, January 2010, pp. 72-81.

[5] C.D. Cuntan, I. Baciu, G.N. Popa, A. Iordan, Study of the deforming regime introduced in the power supply grid by the electric locomotives equipped with DC motors, *WSEAS Transactions on Systems*, Vol. 9, No.8, August 2010, pp. 854-864.

[6] A. V. Doroshin, F. Neri, Open research issues on Nonlinear Dynamics, Dynamical Systems and Processes, *WSEAS Transactions on Systems*, Vol. 13, 2014, in press.

[7] C. Ciufudean, F. Neri, Open research issues on Multi-Models for Complex Technological Systems, *WSEAS Transactions on Systems*, Vol. 13, 2014, in press.

[8] F. Neri, Open research issues on Computational Techniques for Financial Applications, *WSEAS Transactions on Systems*, Vol. 13, 2014, in press.

[9] F. Neri, Open research issues on Advanced Control Methods: Theory and Application, *WSEAS Transactions on Systems*, Vol. 13, 2014, in press.

[10] P. Hájek, F. Neri, An introduction to the special issue on computational techniques for trading systems, time series forecasting, stock market modeling, financial assets modeling, *WSEAS Transactions on Business and Economics*, Vol. 10, No. 4, 2013, pp. 201-292.

[11] Z. Bojkovic, F. Neri, An introduction to the special issue on advances on interactive multimedia systems, *WSEAS Transactions on Systems*, Vol. 12, No. 7, 2013, pp. 337-338.

[12] C. Guarnaccia, F. Neri, An introduction to the special issue on recent methods on physical polluting agents and environment modeling and simulation, *WSEAS Transactions on Systems*, Vol. 12, No. 2, 2013, pp. 53-54.

[13] F. Neri, An introduction to the special issue on computational techniques for trading systems, time series forecasting, stock market modeling, and financial assets modeling, *WSEAS Transactions on Systems*, Vol. 11, No. 12, 2012, pp. 659-660.

[14] M. Muntean, F. Neri, Foreword to the special issue on collaborative systems, *WSEAS Transactions on Systems*, Vol. 11, No.11, 2012, p. 617.

[15] L. Pekař, F. Neri, An introduction to the special issue on time delay systems: Modelling, identification, stability, control and applications, *WSEAS Transactions on Systems*, Vol. 11, No. 10, 2012, pp. 539-540.

[16] C. Volos, F. Neri, An introduction to the special issue: Recent advances in defense systems: Applications, methodology, technology, *WSEAS Transactions on Systems*, Vol. 11, No. 9, 2012, pp. 477-478.

[17] H. Farooq, C. Zhou, M. E. Farrag, Analyzing the Harmonic Distortion in a Distribution System Caused by the Nonlinear Residential Loads, *International Journal of Smart Grid and Clean Energy*, Vol. 2, No. 1, January 2013, pp. 46-51.

[18] H. E. Mazin, E. E. Nino, W. Xuand J. Yong, A Study on the Harmonic Contributions of Residential Loads, *IEEE Transactions on Power Delivery*, Vol. 26, No. 3, July 2011, pp. 1592-1599.

[19] J.A. Pomilio, S. M. Deckmann, Characterization and Compensation of Harmonics and Reactive Power of Residential and Commercial Loads, *IEEE Transactions on Power Delivery*, vol. 22, No. 2, April 2007, pp. 1049-1055.

[20] M. Panoiu, F. Neri, Open research issues on Modeling, Simulation and Optimization in Electrical Systems, *WSEAS Transactions on Systems*, Vol. 13, 2014, in press.

[21] M. Azzouzi, F. Neri, An introduction to the special issue on advanced control of energy systems, *WSEAS Transactions on Power Systems*, Vol. 8, No. 3, 2013, p. 103.

[22] T.G. Ionescu, O. Pop, *Engineering of Power Electrical Distribution*, Bucharest, Romania, Technical Publishing House, 1998 (in Romanian).

[23] J. Meyer, P. Schegner, K. Heidenreich, Harmonic Summation Effects of Modern Lamp Technologies and Small Electronic Household Equipment, *21st International Conference on Electricity Distribution*, Frankfurt, 6-9 June 2011, pp.1-4.

[24] A. Dolara, S. Leva, Power Quality and Harmonic Analysis of End User Devices, *Energies*, Vol. 5, No. 12, December 2012, pp. 5453-5466.

[25] Y.-J. Wang, R. M. O'Connell, G. Brownfield, Modeling and Prediction of Distribution System Voltage Distortion Caused by Nonlinear Residential Loads, *IEEE Transactions on Power Delivery*, Vol. 16, No. 4, October 2001, pp. 744-751.

[26] A. Mansoor, W. M. Grady, P. T. Staats, R. S. Thallam, M. T. Doyle, and M. J. Samotyj, Predicting the Net Harmonic Currents Produced by Large Numbers of Distributed Single-Phase Computer Loads, *IEEE Trans. Power Delivery*, Vol. 10, October 1995, pp. 2001–2006.

[27] ***, Three Phase Power Quality Analyzer CA 8334B, User's Guide, Chauvin-Arnoux, France, 2007.

[28] IEC EN 61000-3-2: *Electromagnetic Compatibility, Part 3, Section 2, Limits for Harmonic Current Emissions (Equipment Input Current ≤16 A per Phase)*, ed. 3; International Electrotechnical Commission (IEC), Geneva, Switzerland, 2011.

[29] ***, *IEEE Std 1459-2010, Definitions for the Measurement of Electric Power Quantities Under Sinusoidal, Nonsinusoidal, Balanced, or Unbalanced Conditions*, February 2010 (Revision of IEEE Std 1459-2000).

[30] P. J. Moore, I. E. Portugués, The Influence of Personal Computer Processing Modes on Line Current Harmonics, *IEEE Transactions on Power Delivery*, Vol. 18, No. 4, October 2003, pp. 1363-1368.

[31] D. O. Koval, C. Carter, Power Quality Characteristics of Computer Loads, *IEEE Trans. Ind. Applicat.*, Vol. 33, May/June 1997, pp. 613–621.

[32] L. Pekař, F. Neri, An introduction to the special issue on advanced control methods: Theory and application, *WSEAS Transactions on Systems*, Vol. 12, No. 6, 2013, pp. 301-303.

[33] P. Karthikeyan, F. Neri, Open research issues on Deregulated Electricity Market: Investigation and Solution Methodologies, *WSEAS Transactions on Systems*, Vol. 13, 2014, in press.

Power Consumption Optimization Strategy of Cloud Workflow Scheduling Based on SLA

YONGHONG LUO, SHUREN ZHOU
School of Computer and Communication Engineering
Changsha University of Science and Technology
960, 2nd Section, Wanjiali South RD, Changsha, Hunan
CHINA
luoyonghong_km@163.com, zsr_hn@163.com

Abstract: -Cloud computing, as a new model of service provision in distributed computing environment, faces the great challenge of energy consumption because of its large demand for computing resources. Choosing improper scheduling method to execute cloud workflow tends to result in the waste of power consumption. In order to lower the higher power consumption for cloud workflow executing, we propose a power consumption optimization algorithm for cloud workflow scheduling based on SLA (Service Level Agreement), which can reduce power consumption while meeting the performance-based constraints of time and cost. The algorithm first searches for all feasible scheduling solutions of cloud workflow application with critical path, then the optimal scheduling solution can be found out through calculating total power consumption for each feasible scheduling solution. The experimental results show that compared with traditional workflow scheduling algorithms based on QoS, the optimization algorithm proposed in this paper not only meets the constraints of time and cost defined in SLA, but also reduces the average power consumption by around 10%.

Key-Words: - Cloud computing, Cloud workflow, SLA, Critical path, Scheduling solutions, Power consumption optimization

1 Introduction

Due to integrating a large number of computing resources and storage resources in cloud data center, cloud computing system needs to solve various problems to implement a high effective, low-cost and safe distributed computing platform [1]. The high power consumption [2, 3] is one of the most serious problems for cloud computing system. According to statistics, the power consumption of cloud data centers [4] has risen by 56 percent from 2005 to 2010, and in 2010 accounted to be between 1.1 and 1.5 percent of the global electricity use [5]. There exists power consumption waste caused by improper scheduling method in addition to the necessary power consumption for executing user tasks in cloud computing system [6]. Cloud computing system usually contains a lot of computers with different performance which may need different response time and power consumption to execute the same tasks. With regard to power consumption, the mismatched scheduling solution [7] usually spends higher power consumption to finish user required task which can be executed with lower power consumption. Therefore, how to realize cloud computing system with low power consumption through scheduling resources appropriately have been widely concerned.

Cloud workflow [8, 9] is a new application mode for workflow management system in cloud

computing environment, which can provide optimization solutions for cloud computing system to reduce operation cost and improve the quality of cloud services [10]. The scheduling of cloud workflow which is the same as that of grid workflow [11] is the problem of mapping each task to a suitable resource and of ordering the tasks on each resource to satisfy some performance criterion [12,13]. The scheduling algorithm of workflow can be divided into two categories: scheduling algorithms based on best-effort service and scheduling algorithms based on OoS constraints [14]. Yu et al. [15] proposed economy-based methods to handle large-scale grid workflow scheduling under deadline constraints, budget allocation, and QoS. Dogan and Özgüner [16] developed a matching and scheduling algorithm for both the execution time and the failure probability that can trade off them to get an optimal selection. Moretti et al. [17] suggested all of the pairs to improve usability, performance, and efficiency of a campus grid.

At present, there are a few works addressing cloud workflow scheduling. Juve in literature [18] compared the performance of running some scientific workflows on the NCSA's Abe cluster, against the Amazon EC2. Both use Pegasus [19] as the workflow management system to execute the workflows. Prodan et al. [20] proposed a bi-criteria scheduling algorithm that follows a different approach to the optimization problem of two arbitrary independent criteria, e.g. execution time and cost. "RC2" algorithm [21] for scheduling tasks in hybrid cloud was proposed by Lee and Zomaya to achieve reliable completion. An initial schedule is first calculated based on private cloud (or locally owned resources) to minimize cloud resource usage. In 2011, Bittencourt and Madeira proposed the "HCOC" algorithm [22] to schedule cloud workflows within deadline while minimizing compute cost. In addition to task execution time and compute cost that are used in the techniques described so far, the "PBTS" algorithm proposed by Byun et al. [23] begins to consider other aspects in the cloud.

So far, there are few works solving energy-aware cloud workflow scheduling. Regarding the existing energy consumption models [24, 25, 26], they all consider only two levels of energy consumption in a machine corresponding to its idle and full-load states. These models, however, do not properly reflect the current energy-aware multi-core architectures. Authors in literature [27] proposed an energy-aware heuristic scheduling for data-intensive workflows in virtualized datacenters, which introduces a novel heuristic called Minimal Data-Accessing Energy Path for scheduling data-intensive workflows aiming to reduce the energy consumption of intensive data accessing. Pareto-based multi-objective workflow scheduling algorithm was proposed in literature [28, 29], which captures the real behavior of energy consumption in heterogeneous parallel systems based on empirical models.

We can know from the aforementioned scheduling algorithms of workflow applications that regardless of time optimization algorithms, cost optimization algorithms scheduling or energy-aware scheduling algorithms for workflow applications, all of them have not effectively solved the power consumption optimization problem faced in the cloud computing environment, which likely result in power waste phenomenon as mismatch scheduling of cloud workflows. So, we propose a power consumption optimization algorithm of cloud workflow scheduling based on service level agreement which tries to match each task of workflow application to the reasonable service provided by server in cloud computing system. The key of optimization algorithm proposed in this paper is to find out all feasible scheduling solutions for candidate cloud workflow applications.

2 Cloud workflow model

2.1 DAG model of cloud workflow

The DAG (Directed Acyclic Graph) is a well-known model for describing workflow applications in

different computing environments. So, a cloud workflow application also can be represented by the DAG G=(T,E) (as shown in fig.1), where T is a set of tasks t_i (i=1,2,…,n), and E is a set of edges $e_{i,j}(t_i \neq t_j)$ that describe the dependencies between tasks. In given DAG model for a cloud workflow, if $t_a \in T$ and $e_{i,a} \notin E$ for all $t_i \in T$, then the task t_a is called an entry task of the cloud workflow; if $t_z \in T$ and $e_{z,i} \notin E$ for all $t_i \in T$, then the task t_z is called a exit task of the cloud workflow. In order to better understand the DAG model, we always add two dummy tasks of t_{entry} and t_{exit} to the beginning and end of the cloud workflow, respectively.

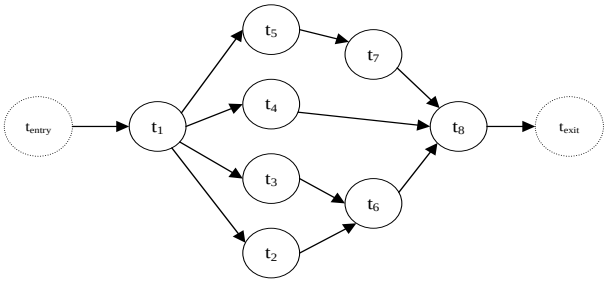

Fig.1 DAG model of a cloud workflow

The service providers offer several services with different QoS for each task of every cloud workflow. We assume that each task t_i of cloud workflow can be executed by k services with different QoS attributes, $S_i = \{s_{i,1}, s_{i,2},\ldots, s_{i,k}\}$. There are many QoS attributes for services in cloud computing system, including execution time, cost, reliability, power energy efficiency, and so on. In this paper, we consider the most important three factors: execution time, cost and power energy efficiency for our scheduling model. $ET(t_i, s_{i,j})$ and $EC(t_i, s_{i,j})$ are defined as the execution time and the execution cost of executing task t_i on service $s_{i,j}$, respectively. The data transfer time of a dependency $e_{i,j}$ only depends on the amount of data to be transferred between corresponding tasks, and it is independent of the services which execute them [30]. Therefore, $TT(e_{i,j})$ is defined as the data transfer time of a dependency $e_{i,j}$, and independent of the selected services for t_i and t_j.

2.2 Critical path for cloud workflow

A schedule of cloud workflow application is defined as an assignment of services to the cloud workflow tasks. If $SS(t_i)$ denotes the selected service for task t_i, then a schedule of cloud workflow w(T , E) can be defined as:

$$\mathrm{Sched}(w) = \{SS(t_i) \mid \forall t_i \in T\ SS(t_i) = s_{i,j} \in S_i\} \quad (1)$$

Definition 1.Service Graph: SG=(S,D), where $S=\{s_i|\ \mathrm{mapping}(s_i,t_i)\}$ is a set of services which include all selected services for each task in cloud workflow application, $D=\{e_{i,j}|(s_i,s_j) \Leftrightarrow (t_i,t_j)\}$ is a set of edges between services (each edge describes a dependency between services in Service Graph). In this paper, a feasible scheduling solution for cloud workflow application is represented as the corresponding service graph. For example, cloud workflow application in figure 1 is scheduled to form mappings between tasks and services as follows: $t_1 \rightarrow s_{1,3}$, $t_2 \rightarrow s_{2,2}$,$t_3 \rightarrow s_{3,4}$, $t_4 \rightarrow s_{4,6}$,$t_5 \rightarrow s_{5,6}$, $t_6 \rightarrow s_{6,8}$, $t_7 \rightarrow s_{7,8}$, $t_8 \rightarrow s_{8,1}$, and its corresponding service graph can be obtained(as shown in fig.2).

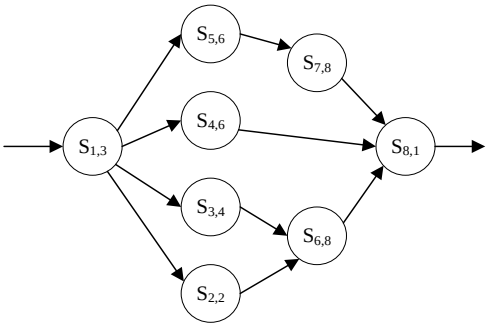

Fig.2 Service graph of a cloud workflow application

Definition 2.Critical path: For any cloud workflow application established workflow model with directed acyclic graph w(T, E), each task is matched to a suitable service during the scheduling. All of mappings between services and tasks can generate a service graph in accordance with w(T,E) of the cloud workflow application, which includes a corresponding critical path denoted as WCP in this paper.

With the WCP of cloud workflow application,

the executive time of cloud workflow application can be defined as:

$$T = \sum_{t_i \in WCP} (ET(SS(t_i)) + TT(SS(t_i))) \quad (2)$$

As for the total cost of cloud workflow application execution, it can be calculated as follows:

$$C = \sum_{i=1}^{n} Cost(SS(t_i)) \quad (3)$$

In order to meet the time constraint of cloud workflow scheduling, we need to define its earliest start time EST, earliest finish time EFT and latest finish time LFT for each task of cloud workflow application. Due to the earliest start time of task t_i at which t_i can start its computation, EST of t_i can be computed as follows:

$$\mathrm{EST}(t_{\mathrm{entry}}) = 0 \quad (4)$$

$$\mathrm{EST}(t_i) = \max_{t_p \in predecessors(t_i)} \{EST(t_p) + ET(t_p, SS(t_p)) + TT(e_{p,i})\} \quad (5)$$

Accordingly, the earliest finish time of each task t_i is the earliest time at which t_i can finish its computation, the EFT of t_i is computed as follows:

$$\mathrm{EFT}(t_i) = \mathrm{EST}(t_i) + \mathrm{ET}(t_i, \mathrm{SS}(t_i)) \quad (6)$$

The latest finish time of task t_i is the latest time at which t_i can finish its computation, such that the whole cloud workflow can finish before the user defined deadline, D. LFT of t_i can be computed as follows:

$$\mathrm{LFT}(t_{\mathrm{exit}}) = \mathrm{D} \quad (7)$$

$$\mathrm{LFT}(t_i) = \min_{t_c \in successors(t_i)} \{LFT(t_c) - ET(t_c, SS(t_c)) - TT(e_{i,c})\} \quad (8)$$

Definition 3.Critical parent: the critical parent of node t_i is the unscheduled parent of t_i that has the latest data arrival time at t_i, that means it is the parent t_p of t_i, for which EST (t_p) + ET (t_p, SS(t_p)) + TT ($e_{p,i}$) is maximal.

The algorithm obtaining critical path for cloud workflow scheduling is as follows:

Input: w(T,E)
Output: WCP
Begin
Step1: add t_{entry}, t_{exit} and their corresponding dependencies to w;
Step2: for (i=1;i<=n;i++) do
Step3: Select the fastest idle service for each task t_i: SS(t_i);
Step4: end for
Step5: for (i=1;i<=n;i++)
Step6: compute EST(t_i) according to Eq. (5);
Step7: end for
Step8: for (i=n;i<=1;i--)
Step9: compute LFT(t_i) according to Eq. (8);
Step10: end for
Step11: mark t_{entry} and t_{exit} as scheduled nodes;
Step11: t=t_{exit}, WCP=null;
Step12: while (there exists an unscheduled parent of t) do
Step15: add CriticalParent(t) to the beginning of WCP;
Step16: t=CriticalParent(t);
Step17: end while
End.

3 Power consumption model

For the power consumption of any cloud workflow which is composed of n tasks during the execution, we can build the following model:

$$PC = \sum_{i=1}^{n} P(t_i, SS(t_i) \times T(t_i, SS(t_i)) \quad (9)$$

Where PC denotes the total power consumption of cloud workflow execution, SS(t_i) represents the selected service for task t_i, P(t_i, SS(t_i)) indicates the power which is needed to execute task t_i on service SS(t_i), T(t_i, SS(t_i)) denotes the time that is spent to execute task t_i on service SS(t_i).

In this paper, we assume that the task set of cloud computing system is W={w_1,w_2,…,w_m}(m>=n), and the arrival rate for each type of cloud task is denoted as λ_i(i=1,2,…,m).

Each service can establish a queuing model of M/M/1 to process a kind of user task requirement, $s_{i,j}$ means that the service selected for task w_i is deployed on the server h_j. So, the arrival rate $\lambda_{i,j}$ of task w_i allocated to h_j can be represented as follows:

$$\lambda_{i,j} = P_{i,j} \times \lambda_i \tag{10}$$

Where $P_{i,j}$ represents the probability for $s_{i,j}$ deployed on server h_j to execute task t_i. If the service rate for service $s_{i,j}$ to reply task t_i is $\mu_{i,j}$, the average response time ART of executing t_i on $s_{i,j}$ can be calculated as follows:

$$ART = \frac{1}{\mu_{i,j} - \lambda_{i,j}} \tag{11}$$

If the time constraint of task w_i is qt_i, then $\mu_{i,j}$ can be expressed as follows in the case of ART=qt_i:

$$\mu_{i,j} = \lambda_{i,j} + \frac{1}{qt_i} = P_{i,j} \times \lambda_i + \frac{1}{qt_i} \tag{12}$$

The service intensity for server h_j to execute all m types of task (w_1, w_2,…, w_m) can be expressed as follows:

$$\rho_j = \sum_{i=1}^{m} \frac{\lambda_{i,j}}{\mu_{i,j}} = \sum_{i=1}^{m} \frac{P_{i,j} \times \lambda_i}{P_{i,j} \times \lambda_i + \frac{1}{qt_i}} \tag{13}$$

The power of any service $s_{i,j}$ at the moment of t denotes as $Power_{i,j}$ can be calculated as follows:

$$Power_{i,j}(t) = P^c + a_{i,j} \rho_j(t)^{b_{i,j}} \tag{14}$$

Where P^c is constant power consumption of service $s_{i,j}$, $a_{i,j}$ and $b_{i,j}$ are power parameters. Generally, different service intensity corresponds to different power parameters. With Eq. (13), the power of server h_j for $s_{i,j}$ can be computed as follows when the workload of service $s_{i,j}$ tends to stability:

$$Power_j = \begin{cases} P^c + a_{i,j} \times \left(\sum_{i=1}^{m} \frac{P_{i,j} \times \lambda_i}{P_{i,j} \times \lambda_i + \frac{1}{qt_i}}\right)^{b_{i,j}}, 0 < \lambda_{i,j} \le \max(\lambda_{i,j}) \\ 0, \lambda_{i,j} = 0 \end{cases} \tag{15}$$

Therefore, we assume that the start time and the end time for service $s_{i,j}$ are represented as $time_1$ and $time_2$,respectively. Then, the power consumption during the execution of service $s_{i,j}$ can be calculated as follows:

$$PC_{i,j} = \int_{time_1}^{time_2} \left(P^c + a_{i,j} \times \left(\sum_{i=1}^{n} \frac{P_{i,j} \times \lambda_i}{P_{i,j} \times \lambda_i + \frac{1}{qt_i}}\right)^{b_{i,j}}\right) dt \tag{16}$$

4 Optimization of power consumption

4.1 Model of power optimization

According to the model of power consumption in this paper, power consumption optimization of cloud workflow scheduling aims to reduce the total power consumption of cloud workflow execution based on the constraints of time and cost in Service Level Agreement, and its optimization model is represented as follows:

$$\begin{cases} \min \sum_{i=1}^{n} P(SS(t_i), t_i) \\ \sum_{t_i \in WCP} Time(SS(t_i), t_i) \le makspan \\ \sum_{i=1}^{n} C(SS(t_i), t_i) \le Cost \end{cases} \tag{17}$$

Where $P(SS(t_i),t_i)$ denotes the power consumption which is produced by executing task t_i on matched service $SS(t_i)$, $Time(SS(t_i),t_i)$ denotes the time is needed to execute t_i on selected service $SS(t_i)$, makspan represents the total time constraint specified in user's Service Level Agreement, $C(SS(t_i),t_i)$ represents the required cost that is necessary to execute task t_i with allocated service $SS(t_i)$, Cost indicates the total cost defined in user's Service Level Agreement.

Definition 4.Feasible Scheduling Solution: if a scheduling solution corresponding to a services graph can finish the execution of cloud workflow w(T,E) successfully while meeting the required time attribute and cost attribute in user's Service Level

Agreement, we call it a feasible scheduling solution. We assume that Sch_k is a feasible scheduling solution for cloud workflow w(T,E) that can satisfy the time attribute and cost attribute in user's Service Level Agreement, Ω(Sch) is the set of all feasible scheduling solution for cloud workflow w(T,E). For any cloud workflow application, we suppose there should be at least one feasible scheduling solution, and let |Ω(Sch)|=L where L represents the number of feasible scheduling solutions. The power consumption which is needed to execute a feasible scheduling solution can be estimated as follows:

$$PC(FSS_k) = \sum_{s_{i,j} \in S_k} PC_{i,j}, FSS_k = (S_k, D_k) \quad (18)$$

4.2 Algorithm of power consumption optimization

In order to solve the problem of power waste caused by the improper scheduling of cloud workflow, the algorithm idea of power consumption optimization for cloud workflow scheduling is as follows: Firstly, algorithm needs to search for all feasible scheduling solutions among the corresponding service graphs of cloud workflow scheduling. For a scheduling solution of cloud workflow application, if its execution time and execution cost obtained by evaluation are all less than the time constraint and cost constraint in SLA, we can mark the solution as a feasible scheduling solution. Then, the power consumption for each feasible scheduling solution can be computed according to Eq.(18). Finally, we select the scheduling solution with the minimum power consumption as the optimal scheduling solution. The detailed algorithm of power consumption optimization for cloud workflow scheduling (PCOA) is as follows:

Input: DAG of cloud workflow, SG

Output: optimal scheduling solution of cloud workflow with the minimum power consumption

Begin

Step1 :K=0;

Step2 :for each SG_i of cloud workflow do

Step3 : Find out the critical path for the SG_i;

Step4 : if ($\sum_{s_i \in WCP} Time(mapping(s_i, t_i)) \le makspan$ and $\sum_{i=1}^{n} C(s_i, t_i) \le Cost$) then

Step5 : add SG_i to FSS_k(feasible schedule solution set);

Step6 : k++;

Step7 : end if

Step8 :end for

Step9 :compute the power consumption of FSS_0 according to Eq.(16);

Step10:min_PC=PC(FSS_0);

Step11:for (j=1; j<k; j++) do

Step12: compute the power consumption of FSS_j according to Eq.(18);

Step13: if (min_PC>PC(FSS_i)) do

Step14: min_PC= PC(FSS_i);

Step15: set FSS_i as the optimal schedule solution of cloud workflow;

Step16: end if

Step17:end for

End.

5 Experimental results and analysis

To evaluate the effectiveness of power consumption optimization strategy for cloud workflow scheduling proposed in this paper, we employed three workflow scheduling methods including Loss and Gain, Deadline-MDP and PCOA to carry out four scientific workflow applications , such as Montage, Epigenomics, MRI and e-protein in simulated cloud computing environment CloudSim, and compared the time, cost and power consumption for them after Loss and Gain, Deadline-MDP and PCOA finished the execution of Montage, Epigenomics, MRI and e-protein. In experiment, we assigned a time constraint (Montage:400s, Epigenomics:400s, MRI:350s, e-protein:350s) and a cost constraint (Montage:35$, Epigenomics:35$, MRI:30$, e-protein:30$) for each cloud workflow application, which are represented as makspan and cost,

respectively. Moreover, we also provided ten services for each type of task, which are deployed on different servers. All of ten services need to spend different time and cost to process the same task. Generally speaking, a faster service costs more power than a slower one. Environment parameters involved in this experiment and their values are shown in table 1.

After completing ten times execution for each scientific workflow application, the average time, cost and power consumed by three different scheduling methods are shown in fig.3, fig.4 and fig.5, respectively. Fig.3 shows that under the constraints of time and cost in SLA, Loss and Gain method performs each workflow application with the least time, and Deadline-MDP spends the most time to finish the execution of every workflow application, while the run time for PCOA is greater than that of Loss and Gain, and less than that of Deadline-MDP. So, we should adopt Loss and Gain method to schedule various workflow applications if the target of scheduling cloud workflow is to minimize the completion time.

Table 1.Parameters setting of the simulated environment

Parameter	Setting	Description
h	25	Number of servers in simulated cloud environment
λ_i	[5,20]	Average arrival rate for task t_i(i=1,2,…)
$\mu_{i,j}$	[4,15]	Serving rate for server h_j to execute task t_i
P_j	[50w,80w]	Idle power of server h_j
$P_{i,j}$	[200w,600w]	Executive power of server h_j processing task t_i
makspan	[50s-400s]	Time constraint in user's SLA
cost	[10-50]	Cost constraint in user's SLA

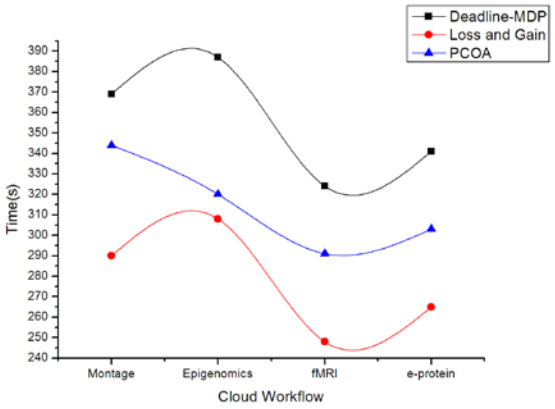

Fig.3 Comparison of average time for performing cloud workflow

Fig.4 indicates that with the constraints of time and cost in SLA, Loss and Gain method needs to spend the highest cost to execute each of workflow applications and Deadline-MDP only spends the lowest cost to perform every workflow application, while the average cost for PCOA to finish the execution of all workflow applications is slightly lower than that of Loss and Gain method. Therefore, we should select Deadline-MDP method if the scheduling aims to minimize the cost of cloud workflow execution.

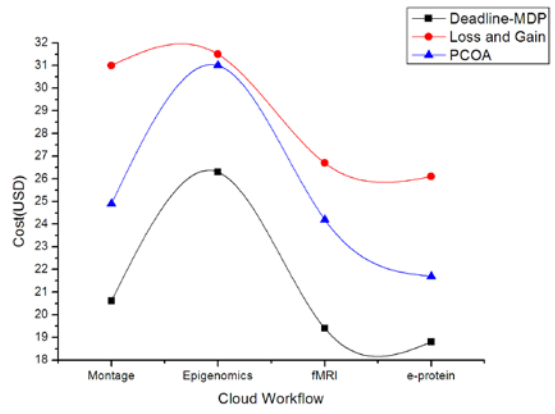

Fig.4 Comparison of average cost for performing cloud workflow

We can know from fig.5 that under the constraints of time and cost in SLA, Deadline-MDP, Loss and Gain spend almost the same power to complete the execution of each workflow application, while the average power consumption produced by PCOA is the optimal among the three scheduling

methods of Loss and Gain, Deadline-MDP and PCOA. The reason why PCOA can reduce the power consumption of cloud workflow application execution is that PCOA can select the optimal scheduling solution for each cloud workflow application through using critical path. The experimental results show that compared with traditional workflow scheduling algorithms based on QoS, the optimization algorithm proposed in this paper not only meets the constraints of time and cost defined in SLA, but also reduces the average power consumption by around 10%. So, we should employ PCOA to dispatch all cloud workflow applications in order to reduce the power consumption of cloud workflow execution caused by improper scheduling algorithm in cloud computing environment.

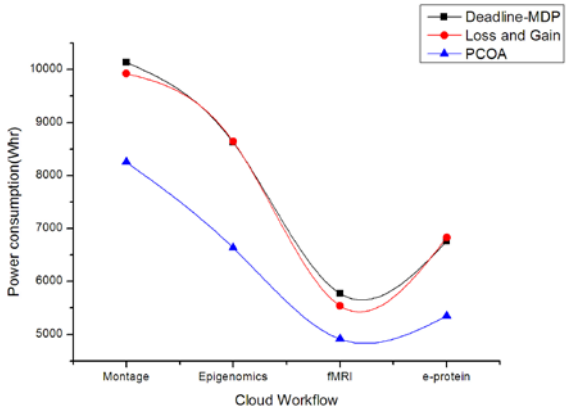

Fig.5 Comparison of average power consumption for performing cloud workflow

6 Conclusions

This paper studied the power consumption optimization of cloud workflow scheduling as energy waste issues in the cloud computing environment have become increasingly prominent. Through analyzing the power computing model for cloud workflow application execution, we have proposed a power consumption algorithm of cloud workflow scheduling under the constraints of time and cost in SLA. Simulated experiments demonstrate that this optimization method is fully effective and feasible. But the power optimization issue isn't implemented in the virtual cloud environment. So, we will further investigate the power consumption optimization of cloud workflow scheduling based on the virtual machines allocation in the future, and carry out experiments in real virtualization cloud platform so as to ensure the correctness and effectiveness of research result.

Acknowledgements

This work was supported by National Natural Science Foundation of China (Grant no. 51277015) and Scientific Research Fund of Hunan Provincial Education Department (Grant no. 13C1003).

References:

[1] Doroshin, A. V., Neri, F, Open research issues on Nonlinear Dynamics, Dynamical Systems and Processes, WSEAS Transactions on Systems, Vol.13, 2014, in press.

[2] Azzouzi, M., Neri, F., An introduction to the special issue on advanced control of energy systems , WSEAS Transactions on Power Systems, Vol.8, No.3 , 2013, p. 103.

[3] Yiming Tan, Guosun Zeng, Wei Wang, Policy of Energy Optimal Management for Cloud Computing Platform with Stochastic Tasks, Journal of software, Vol.23, No.2, 2012, pp.266-278. (In Chinese)

[4] Armbrust M, Fox A, Griffith R, Joseph A D, A view of cloud computing, Communications of the ACM, Vol.53, No.4, 2010, pp.50-58.

[5] Karthikeyan, P., Neri, F, Open research issues on Deregulated Electricity Market: Investigation and Solution Methodologies, WSEAS Transactions on Systems, Vol.13, 2014, in press.

[6] Ciufudean, C., Neri, F, Open research issues on Multi-Models for Complex Technological Systems, WSEAS Transactions on Systems, Vol.13, 2014, in press.

[7] Chuang Lin, Yuan Tian, Min Yao, Green Network and Green Evaluation: Mechanism, Modeling and Evaluation, Chinese Journal of

Computers, Vol.34, No.4, 2011, pp.593-612.
[8] Xuezhi Chai, Jian Cao, Cloud Computing Oriented Workflow Technology, Journal of Chinese Computer Systems, Vol.33, No.1, 2012, pp. 90-95.
[9] Dong Yuan, Yun Yang, Xiao Liu, Gaofeng Zhang, Jinjun Chen, A data dependency based strategy for intermediate data storage in scientific cloud workflow systems, Concurrency and Computation: Practice & Experience, Vol.24, No.9, 2012, pp.956-976.
[10] Panoiu, M., Neri, F, Open research issues on Modeling, Simulation and Optimization in Electrical Systems, WSEAS Transactions on Systems, Vol.13, in press.
[11] Haijun Cao, Hai Jin, Xiaoxin Wu, Song Wu, ServiceFlow: QoS-based hybrid service-oriented grid workflow system, Journal of Supercomputing. Vol.53, No.3, 2010, pp. 371-393.
[12] S. Abrishami,M. Naghibzadeh, Deadline-constrained workflow scheduling in software as a service Cloud, Scientia Iranica, Vol.19, No.3, 2012, pp.680-689.
[13] Neri, F, Open research issues on Advanced Control Methods: Theory and Application, WSEAS Transactions on Systems, Vol.13, 2014, in press.
[14] Jia Yu, Rajkumar Buyya, A Taxonomy of Workflow Management Systems for Grid Computing, Journal of Grid Computing, Vol.3, No.3-4, 2005, pp.171-200.
[15] J. Yu, R. Buyya, Scheduling scientific workflow applications with deadline and budget constraints using genetic algorithms, Scientific Programming Journal, Vol.14, No.1, 2006, pp.217–230.
[16] A. Dogan, F. Özgüner, Biobjective scheduling algorithms for execution time–reliability trade-off in heterogeneous computing systems, The Computer Journal, Vol.48, No.3, 2005, pp. 300–314.
[17] C. Moretti, H. Bui, K. Hollingsworth, B. Rich, All-pairs: an abstraction for data-intensive computing on campus grids, IEEE Transactions on Parallel and Distributed Systems, Vol.21, No.1, 2010, pp. 33–46.
[18] Ewa Deelman, Grids and Clouds: making workflow applications work in heterogeneous distributed environments, International Journal of High Performance Computing Applications, Vol.24, No.3, 2010, pp. 284–298.
[19] Ewa Deelman, Gurmeet Singh, Meihui Su, Pegasus: a framework for mapping complex scientific workflows onto distributed systems, Scientific Programming, Vol.13, No.3, 2005, pp. 219–237 .
[20] Prodan R, Wieczorek M, Bi-criteria scheduling of scientific grid workflows, Automation Science and Engineering, Vol.7, No.2, 2010, pp. 364–376.
[21] Y. C. Lee, A. Y. Zomaya, Rescheduling for reliable job completion with the support of clouds, Future Generation Computer Systems, Vol.26, 2010, pp. 1192-1199.
[22] L. F. Bittencourt, E. R. M. Madeira, HCOC: A Cost Optimization Algorithm for Workflow Scheduling in Hybrid Clouds, Journal of Internet Services and Applications, Vol. 2, 2011, pp. 207-227.
[23] E. Byun, Y. Kee, J. Kim, S. Maeng, Cost optimized provisioning of elastic resources for application workflows, Future Generation Computer Systems, Vol. 27, pp. 1011-1026, 2011.
[24] M. Mezmaz, N. Melab, Y. Kessaci, Y.C. Lee, E.-G. Talbi, A.Y. Zomaya, D. Tuyttens, A parallel bi-objective hybrid meta heuristic for energy-aware scheduling for cloud computing systems, Journal of Parallel and Distributed Computing, Vol.71, 2011, pp. 1497–1508.
[25] P. Lindberg, J. Leingang, D. Lysaker, S.U. Khan, J. Li, Comparison and analysis of eight scheduling heuristics for the optimization of energy consumption and makespan in large-scale distributed systems, Journal of Supercomputing, Vol.59, No.1, 2010, pp. 478–484.
[26] N. Min-Allah, H. Hussain, S.U. Khan, A.Y. Zomaya, Power efficient rate monotonic scheduling for multi-core systems, Journal of Parallel and Distributed Computing, Vol.72, No.1, 2012, pp.48–57.
[27] Peng Xiao, Zhi-Gang Hu, Yan-Ping Zhang, An Energy-Aware Heuristic Scheduling for Data-Intensive Workflows in Virtualized Datacenters, Journal of Computer Science and Technology,

Vol.28, No.6, 2013, pp. 948-961.
[28] Juan J. Durillo, Vlad Nae, Radu Prodan, Multi-objective energy-efficient workflow scheduling using list-based heuristics, Future Generation Computer Systems, Vol.36, 2014, pp.221–236.
[29] Pekař, L., Neri, F, An introduction to the special issue on advanced control methods: Theory and application, WSEAS Transactions on Systems, Vol.12, No.6, 2013, pp. 301-303.
[30] Pekař, L., Neri, F, An introduction to the special issue on time delay systems: Modelling, identification, stability, control and applications, WSEAS Transactions on Systems, Vol.11, No.10, 2012, pp. 539-540.